QUANTUM TRANSPORT AND SWITCHING IN LONG-RANGE COUPLED QUANTUM SYSTEMS

By

Clara Javaherian

A THESIS SUBMITTED TO MACQUARIE UNIVERSITY
FOR THE DEGREE OF DOCTOR OF PHILOSOPHY
DEPARTMENT OF PHYSICS AND ASTRONOMY
JANUARY 2016

© Clara Javaherian, 2016.

Typeset in LaTeX 2_ε.

Except where acknowledged in the customary manner, the material presented in this thesis is, to the best of my knowledge, original and has not been submitted in whole or part for a degree in any university.

Clara Javaherian

Acknowledgements

Thanksgivings

I am thankful to my parents who enlivened my soul and sensitively kept supporting and training me from the beginning. I thank all their wonderful consultations and the brilliant times they made out of some tough durations of my Ph.D. study.

I thank Professor Jason Twamley, my Ph.D. supervisor in Macquarie University, for all great suggestions, highly professional guidance, and the whole time he spent for my projects and degree. In addition, I thank Professor Martin Plenio, my Ph.D. supervisor in Ulm University for the fruitful project and his great helpful discussions.

I also appreciate my Ph.D. scholarships through Alexander von Humboldt Foundation at Ulm University and International Macquarie University Research Excellence Scholarship at Macquarie University.

The degree and thesis characteristics

This is a *thesis by publication* and does not include all achievements or ongoing projects during the Ph.D. study. It contains three main chapters that one is article based with original materials and the other two ones are almost the same as the corresponding published papers.

The Ph.D. degree is awarded by Macquairie University, although the Ph.D. projects were performed at both Ulm University and Macquarie University. The affiliation of Ph.D. publications are to both Universities.

The whole Ph.D. degree took five years including two years in Ulm University and three years in Macquarie University where I continued and promoted the works done at Ulm University. The reports of thesis examiners received in six months and the degree was obtained soon after.

History

My Masters degree was awarded from Shahid Beheshti University (Tehran, Iran) through the supervision of Professor Babak Shokri that was a rich and self-contained three-year program. After the graduation while publishing the results [1–6] I was invited to attend a starting Ph.D. program in Heidelberg University (Heidelberg, Germany). My visa enquiry to Germany coincided a historic event in Iran and lasted for about one year.

The result of a sensitive presidential election in Iran in mid-2009 caused mass protests in Tehran and Iran main cities, so that the streets were occasionally at unrest for about one year. Then the Arab Spring demonstrations started in late 2010 in different countries and ended in 2012. The protests in Syria that started in 2012 turned to a civil war and now people hope it would end through the peace talks.

When I reached Heidelberg University after a year of delay, I was also offered am excellent Ph.D. position at Darmstadt University. Since I had a strong willing to obtain a high quality Ph.D. since my Bachelors degree, and wanted to make an informed decision, I got some valuable and professional consultations from my Bachelors supervisor, A/Professor Ali Rezakhani. Finally, I waited about another half a year to start maybe a more desirable Ph.D. in Ulm University (Ulm, Germany). In the meantime, I enjoyed doing a full-time and successful research in Heidelberg University in the historic city of Heidelberg.

In Ulm University, I worked on several aspects of a problem. My main Ph.D. project was to find a regime including a specific phenomenon i.e. transition within spacial dimensions. The initial amount of the parameter specifying this phenomenon was $O(10^{-3})$ that was found by my Ph.D. supervisor in Ulm, Professor Martin Plenio. I was supposed to find a larger amount of this parameter through search algorithms. During the first year and through our discussions mostly with a postdoctoral researcher at the time, A/Professor Filippo Caruso, we were not able to find any

higher amount of transition. Then, this time alone, but using some useful suggestions of my main supervisor, I was able to increase the parameter for one order of magnitude within six months, and by the next half of the year, using high performance computing taught to me by Doctor Shi Machnes, I showed that the found transition was a global maximum. These results are presented in section 2.1.3 of this thesis and the corresponding appendices. During my study in Ulm, I was expected to agree with a change of supervisor that was not efficient for me and not for what I went to Ulm University. So I found other opportunities to continue and finish my Ph.D. projects. At first, I took a very desired new experience by working for a few months in a Quantum Optics laboratory in Dortmund University (Dortmund, Germany), and then came to Macquarie University (Sydney, Australia), where by the aim of my supervisor, Professor Jason Twamley, I could promote and finish most of my previous projects that are presented in this thesis.

Finally, I acknowledge that I find my Ph.D. study very interesting, and international with lots of branched projects. During the research, I also encountered beautiful graphs. For instance, Fig. 3.6(b) was accepted for the kaleidoscopes of Physical Review A in October 2014, and an artistic version of Fig. 3.1(a) was the people choice of the Quantum Image competition of the Department of Physics and Astronomy of Macquarie University.

Related publications

- C. Javaherian, J. Twamley *Robustness of optimal transport in one dimensional particle quantum networks*. Phys. Rev. A **90**, 042313 (2014)

- C. Javaherian, J. Twamley *Platonic quantum networks as coherence-assisted switches in perfect and imperfect situations*. J. Phys. D: Appl. Phys. **48**, 235104 (2015)

Abstract

Controlling the dynamics of quantum states is a common demand in quantum technology. We theoretically study quantum transport and switching in long-range coupled quantum networks possessing a single excitation. The qubit networks of our study are affected by Markovian environments while one qubit is irreversibly connected to an additional site. Different goals are studied towards controlling quantum transport such as efficient single excitation transfer, switching quantum transport, and manipulating the quantum states of qubit networks. These goals have been previously investigated using different mechanisms, however in this thesis we approach them by proposing appropriate geometrical arrangements of sites.

Regarding efficient single excitation transfer we follow two approaches: Checking if there exist a spatial dimension preference for qubit arrangements towards optimal quantum transport, and whether the efficient network designs are robust against geometrical variations.

For dimension analysis a random walk optimization method is used to compare the transport efficiency of networks expanded in one and two spatial dimensions. We find that for some choices of network parameters the two-dimensional networks are slightly more efficient than the one-dimensional equivalent networks. This assures that designing one-dimensional qubit channels are adequate for efficient transport and the two-dimensional networks should only be considered where the two-dimensional spatial expansion is more compatible with the surrounding architecture. To design a network, after deciding about the network dimensionality, one may attempt to optimize

the channel geometry which might result in a non-robust optimal configuration against the geometrical errors.

To achieve robust optimal configurations we follow two approaches: We investigate the efficient configurations of sites in both one and two dimensional arrangements and present some patterns of robust geometric arrangements of sites in geometrical parameter space. Another approach to achieve robust efficient transport is defining a quantity as the geometrical robustness (geo-robustness) of qubit networks. By optimising geo-robustness against the network-environment parameters one can efficiently transfer a single excitation with many arbitrary arrangements of the network sites.

Switching of quantum states is another goal towards controlled quantum dynamics. We study the transport characteristics of highly symmetric three-dimensional networks and analytically prove that a fraction of the initially injected excitation can trap for long durations via the creation of dark states. Using this characteristic we suggest switching devices which are robust against environmental noises.

Contents

List of Figures

List of Tables

1

Introduction

1.1 Quantum transport and switching in qubit networks

Quantum transport is a key concept for understanding the dynamics of the sub-atomic world. It refers, in general, to the motion of different quantum carriers, especially to electrons in nano-devices [10, 11]. There are different approaches towards studying quantum transport in general or in qubit networks, for instance quantum energy or state transfer has been so far studied in different spatial dimensions in bulk, mesoscopic, and nanometric materials. It is also possible to study quantum transport in different natural or synthetic materials like optical fibres, photonic crystals, and nanoparticles. Another approach to study quantum transport is via the manner by which the

system elements interact with each other and the range of the interactions. This factor can have significant effects on the transport properties. From a modeling point of view, quantum transport in open quantum systems can be often subject to a Markov approximation leading to Markovianity. Moreover, quantum states can be transported through adiabatic passage, i.e. a powerful quantum transport method that has been studied and demonstrated in different implementations of qubits. Quantum transport can be also studied from an application point of view to achieve specific purposes like quantum switches or quantum gates in quantum technology. In this introductory chapter we will review various schemes of quantum transport in qubit networks.

1.1.1 Qubit channels

Arrays of qubits are used to store or transfer quantum states within networks. Quantum channels are particularly used for transporting qubit states by converting them to a photon or a quantum carrier state, evolving the carrier over the channel, and then transferring it to a storage site. In general, a channel is any device taking a quantum system as input and transferring it to a spatially distant quantum system as the output. This may include any processing steps required, like preparation, free and controlled time evolutions, and measurements. Channels thus play a central role in information science. Quantum channels can transmit both classical and quantum information, ideally using pure or entangled quantum states. Channels have a finite capacity measured in bits or qubits per unit time which is the flux of quantum information that can be sent undistorted through the channel. Theoretically, quantum channels are described as complete positive trace-preserving maps between spaces of operators. They map a density matrix of the input system from one Hilbert state to a density matrix in the output Hilbert state, potentially with different rank, while preserving the trace and positivity of the matrix (complete positivity).

Physical implementations of qubit channels vary. They range from arrays of nanoparticles to arrays of trapped ions or neutral atoms, arrays of superconducting qubits, arrays of optical cavities, or arrays of quantum dots. In various platforms, the quantum energy carriers could be optical photons, surface plasmons, electrons, Cooper pairs, or exitons.

A common application of quantum channels is connecting quantum nodes of qubits to create quantum networks. There are different protocols for coupling quantum nodes and channels effectively. Depending on the types of physics involved, for example, to couple a photonic qubit to a solid state qubit one can focus the photon to a smaller region and have it interact strongly with the solid state qubit [12]. Another way is to consider an ensemble of solid state qubits to increase the absorption cross section [13]. Using optical resonators [14] is also a method to increase the efficiency of channel-node coupling as the high Q optical resonator photon qubit enhances the coupling strength. Typically the coupling of channels to nodes is probabilistic due to a variety of manufacturing errors, different environmental noises, and loss.

1.1.2 Quantum energy or state transfer

For quantum transport in general it has been proven that a short qubit array with an isotropic homogeneus Heisenberg interaction is suitable for quantum state transfer [15]. In such protocol, an initial quantum state is prepared at one qubit while the rest of the qubits are in the ground state. After a certain amount of time the state of the last qubit is measured and the fidelity of this state to the initial qubit state determines the efficiency of quantum transport.

There are different methods that are proposed to achieve quantum state or energy transfer with unit fidelity. A special form of the Hamiltonian with spatially varying coupling constants between the qubits allows us to avoid dispersion for perfect quantum state transfer [16, 17]. Another method is to form Gaussian wave packets with low dispersion by encoding the information using multiple spins [18]. Also the combination of two spin chains can be used to achieve perfect state transfer [19] and this approach can be implemented using almost any two spin chains which is stable to fluctuations of the chain parameters [20]. However, the time after which perfect state transfer is achieved grows if the individual fidelities of the chains decrease.

Here we provide some examples of energy excitation transport through different chains of qubits. Arrays of trapped ion qubits are one of the promising systems for quantum transport. Ramm *et al* [7], investigated energy transport in chains of trapped ions. Using pulsed excitation scheme they

rapidly add energy to the local motion mode of one of the ions and prepare the system in an out-of-equilibrium state. The propagation of excitation through the chain is determined via subsequent energy read-outs which show multiple revivals of energy at the end of the chain. Such energy revivals persist for a surprisingly long time indicating that the system does not thermalize on the experimental timescale. The pattern of evolved energy transfer for arrays of $2-37$ trapped ions achieves in compliance with their eigen-energies. Fig. 1.1 shows the schematic and the florescence image of their experiment.

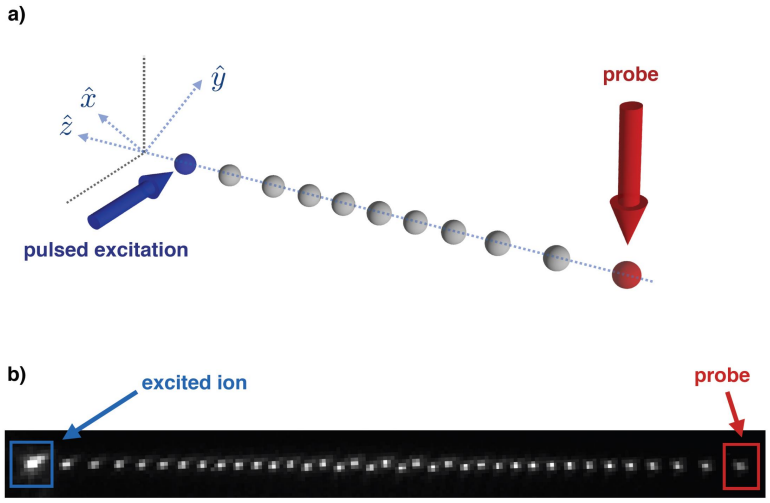

FIGURE 1.1: Fig 1 of ref [7]: (a) The pulsed excitation beam (blue) rapidly adds energy to the ion chain. After a free time evolution, the energy can be read out anywhere along the chain with a probe at $729nm$ (red). Both beams are at 45° with respect to the radial modes of motion. (b) The CCD image of the ion chain with 37 ions with the tightly focused excitation beam.

The propagation of surface plasmon polaritons through a closely spaced metal nanoparticle array could be considered as an example of quantum transport [21] by means of nanoparticle qubits with two distinct states of $|1\rangle$ and $|0\rangle$ at resonance frequency and off-resonance, respectively. A laser pulse is applied to one nanoparticle at its resonance frequency and the evolution of this energy is studied. Via Finite Difference Time Domain simulations Maier et al [8] showed that the electromagnetic pulses at optical frequencies can propagate along short arrays of noble metal nanospheres due to near field interactions of plasmon polariton modes. In addition, the near field microscopy showed experimental evidence for energy propagation over a distance of $0.5\mu m$ of spheroidal silver

particles fabricated using electron beam lithography. Fig. 1.2 shows the energy transport within an array of silver nanorods by presenting the far-field extinction spectrum of Ag nanoparticle chains, and the extinction spectrum of an isolated nanorod, where the extinction of the incoming light is due to the absorption, reflection, or the scattering from the nanoparticles. The inset of Fig. 1.2 is the SEM image of the Ag plasmon waveguide of the nanorods.

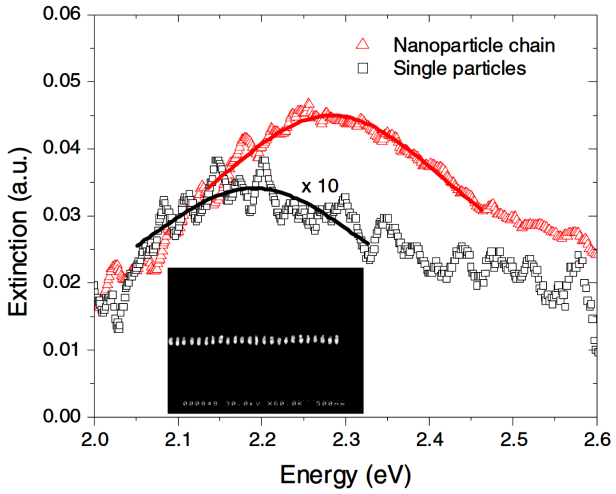

FIGURE 1.2: Fig 4 of ref [8], The far-field extinction spectrum of a plasmon waveguide consisting of Ag nanorods with a 3:1 aspect ratio and a surface-to-surface spacing of 50 nm between adjacent particles shows a plasmon resonance peak shift to higher energies (red triangles and Lorentz fit) compared to the extinction spectrum of isolated, non-interacting particles (black squares and Lorentz fit). The exciting light was polarized along the long axis of the nanorods, perpendicular to the particle chain axis. The inset shows an SEM micrograph of the plasmon waveguide under study.

Another promising chain for quantum state or energy transport is a quantum dot array. In a semiconductor crystallite smaller than its exciton Bohr radius, the excitons are squeezed and confined. The exciton energy levels are discrete as a particle in a box, with energy separation depending on the length of the box. In this regime the electronic and optical properties are highly tunable via size and shape variations. For example, the energy band gap of a quantum dot determines the frequency range of the emitted light which is inversely related to its size. A specific type of quantum dot is lateral quantum dot which is made of a small area of decreased electric potential in a two-dimensional electron gas confined between two semiconductor sheets such as InAs and GaAs. The electric potential is applied to the free electron gas by electrical gates. Individual electrons can

be confined in quantum dots defined by electrostatic gates applied to a two-dimensional electron gas. The gate pattern can be created by electron-beam lithography and measurements would be performed at 50 mK, in a dilution refrigerator. The number of electrons on each dot and the tunnel coupling between dots and from dots to leads can be controlled using gate voltages. In addition, microwave excitation can drive single-spin rotations of trapped electrons, and coherent exchange could be achieved using nanosecond gate voltage pulses [22].

For coherent electron charge transfer within such quantum dots, Braakman *et al* [9] proposed a linear array of three quantum dots where only adjacent dots were connected through tunnel barriers and the left and right dots were also tunnel coupled to the left and right reservoirs, respectively. A scanning electron microscopy (SEM) image of such device is shown in Fig. 1.3. Above the blue shaded gate a charge sensing quantum dot (SQD) is created, the conductance of which is sensitive to the number of charges on each dot through capacitive coupling. The strength of four tunnel couplings can be tuned individually with the voltages on the barrier gates labelled B in Fig. 1.3. This triple dot array is operated in the few electron regime so that by sweeping the voltages on gates LP, MP, and RP (Fig. 1.3) the number of electrons on each of the dots can be changed one by one. By using real time charge detection techniques it was shown that the rate of electron hopping between the outer dots depends on the detunning of the energy levels of the middle site. So coupling within distant sites via tunnel coupling occurs by means of virtual occupation of an intermediate site. The strength of this long distant coherent coupling can be adjusted by energy detuning of the middle site.

1.1.3 Open quantum systems and Markovian regime

Open quantum systems can be studied in Markovian or non-Morkovian regimes. In the Markovian regime the system evolves through a Markovian master equation where the effect of environment is modeled by Lindblad operators. The Lindbladian master equation is obtained by considering Born-Markov approximation by which the system-bath coherence is negligible. In such cases the total density matrix of the system is a tensor product of the density matrices of the system and the

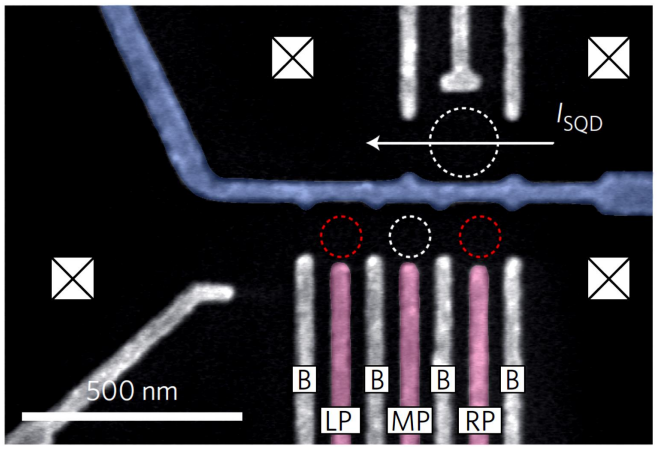

FIGURE 1.3: Fig 1a of ref [9]: SEM image of a sample identical to the one used for the measurements. Dotted circles indicate quantum dots, squares indicate Fermi reservoirs in the 2DEG, which are contacted through ohmic contacts. Both the current through (white arrow) and the reflectance of the SQD are monitored and used to determine the occupancies of the triple quantum dot.

bath [23].

In the non-Markovian regime the dynamics of the quantum system is strongly affected by the structure of the environment. Environmental structure is characterizes by spectral distribution, coherences, the number of excitations and their statistical distribution [24]. There are different methods for studying system dynamics surrounded by a non-Markovian environment. For example, an array of N cavities embedded in a non-Markovian bath has been studied by an exact master equation without approximations derived by quantum state diffusion approach. It is shown that a three coupled cavity array in a highly non-Markovian environment can induce cat-like state transfer, the so-called memory-assisted cat state transfer [25].

In the Markovian regime, quantum transport has been studied for different types of qubit networks within various physical implementations. Population transfer along a qubit network has been also studied in the Markovian regime. In such modeling the first site is initially populated with one energy excitation while all other sites are in their ground states. A target site could be considered at the end of the array which would be dissipatively connected to the last site. It has been shown that for the cases of all-sites equally interacting [26], or nearest neighbor Heisenberg interactions [27],

there is a peak of transported population to the target site as one varies the environmental dephasing noise. This indicates that the efficiency of transport will increase by exposing the qubit systems to dephasing noise. In the absence of dephasing noise the energy is trapped within the network in terms of dark states that neither absorb nor emit the quantum energy. The environment-assisted transport is due to the fact that the dephasing disturbs the energy levels of the system which could trap the initial energy excitation. While each system energy level is fluctuating within a range proportional to the amount of dephasing, new energy paths are provided through the network leading to more efficient transport [26, 28].

The spin conductivity of a spin chain with a tight binding model has been also studied in the Markovian regime. While the chain is connected to two lateral sites through a dissipative process it has been shown that at some dephasing noise rates the conductivity has a single or double maxima [27].

Another example is the photon transfer through a system of four coupled optical cavities. It has been shown that the efficiency of transport can be also improved by including photon path dephasing noise. Numerical simulations for experimentally realistic values represent a substantial enhancement in the photon transport efficiency with environmental dephasing cavity noise [26]. A similar scheme has been also studied on using a network of atoms in suitable ion traps [29].

1.1.4 Adiabatic passage

By completely isolating a quantum system and changing a parameter in the Hamiltonian slowly in time, it can evolve adiabatically from an initial state to a final one remaining in an instantaneous eigenstate. In other words, if the time dependent Hamiltonian of a system varies slowly compared to the energy gap between the eigenstates, the corresponding quantum system remains in an eigenstate.

Different protocols have been already proposed for population transfer by adiabatic passage like Stimulated Raman Adiabatic Passage (STIRAP) [30], Coherent Tunnelling Adiabatic Passage (CTAP) [31], and Dark state Adiabatic Passage (DSAP) [32, 33].

STIRAP is studied for different implementations like a triple array of quantum dots [34]. A routine example of STIRAP is in a three-level Lambda system where population is transferred between two ground energy levels without populating the excited state. To perform it, two laser pulses are applied to the system with frequencies corresponding the gap energies of the two ground states and the excited state. In the case of intuitive transfer, the population of one ground state will be transferred to the excited state via a Rabi π pulse, and then be transferred to the other unpopulated ground state via another Rabi pulse. In the counter-intuitive pulse by optimizing the detunings of laser frequencies from the atomic resonances and the delay time of applying lasers, the population accumulated on one ground state will be transferred to the other ground state while the excited state remains empty during the transfer. So the optimized population transfer with STIRAP is achieved by engineering the detuning frequencies and the time delay [30].

A spatial variant of STIRAP is CTAP which is an adiabatic passage technique to mediate transport through real space rather than phase space. As an example, Jong et al [31] proposed a CTAP device composed of five phosphorous donor sites buried in silicon. They put barrier gates on silicon surface to control the tunnel matrix elements. A counter intuitive alternative gate bias sequence can transport the electron from one end to the other in a robust manner. This structure is extendable to an arbitrary (odd) number of sites. Based on an effective mass treatment they analyse the system and make estimates of the timescale required for the operation of CTAP with the alternating coupling scheme for this device.

CTAP has been studied in many contexts like atoms in triple well potentials [35], electrons bound to quantum dots and donors [36], Bose-Einstein condensates [37], photons in waveguides [38], and Bose-Hubbard systems [39].

Another scheme related to STIRAP is DSAP. The dark state in a three-level-system is an eigenstate of the system and has no overlap with the excited state, which is the eigenstate that is utilized by the STIRAP process. DSAP is named for the multispin generalization of a dark state transfer process. An example of DTAP is a device of three spin-one sites with nearest-neighbor coupling which works by applying a pulse sequence such that in the first half of the transforming procedure

the coupling between the first two sites is much smaller than that of the last two sites, however in the second half of the transport period, the coupling ratios are exchanged. It is then shown that the population in the first site would smoothly transfer to the last site while the the middle site is never populated [32].

1.1.5 Qubit array switches

Besides efficient quantum information transport, manipulating qubit arrays can be used to design quantum devices or elements of quantum circuits. For example switches play an important role in programming quantum transport within networks. There are different proposed switching protocols.

For example, there is a switch made of a superconducting qubit array coupled to a superconducting resonator [40]. Through the nonlinear effects in the many-body state of the qubit array with a semi-classical approach of study, a sudden switching has been observed in the qubit array as a bistable regime between the ferromagnetic phase and the paramagnetic phase. Such phase switchings cause finite energy changes in the qubit array in analogy to a first order phase transition.

Another example of qubit array switching is a network with multiple atomic nodes connected by guided light [41]. A setup has been experimentally demonstrated that strongly couples a photon to a single atom trapped in the near field of a nanoscale photonic crystal cavity. It is shown that the single atom can switch and shift the phase of the coupled photon and on the other hand the photon can modify the phase of atom. Depending on the state of the atom which is controlled by the single photon, a flow of photons can be turned on and off. Such single-photon switch in which a single gate photon controls the propagation of a subsequent probe field can pave the way to integrated quantum nanophotonic networks.

1.1.6 Thesis preview

In this thesis we theoretically study controlled quantum transport in qubit channels. The two main studied approaches are efficient quantum transport and switching the transport within different sites. The channels of interest are qubit arrays in Markovian environments which are initialized in

the ground state and are supposed to transfer a single energy excitation on one site to an irreversibly connected site.

In Chapter 2, to achieve optimal transport of pure quantum states two main approaches are followed: The dimension analysis to check whether there is a spatial dimension preference for optimal quantum transport within dipolar quantum networks, and analysis regarding the robust efficient quantum transport. In the first section, the transport efficiencies of one and two-dimensional qubit networks are compared over a large range of network parameters and it is shown that in some cases the two-dimensional arrangements of qubits transfer the energy in a more efficient manner than the one-dimensional ones. In the second section, we show the patterns of network configurations in the corresponding geometrical parameter spaces for robust efficient transport within one and two-dimensional networks. For instance, it is shown that in few site networks and under specific circumstances the pair and symmetric configurations of dipolar networks can transfer a pure state in a robust manner.

In Chapter 3, towards optimal quantum transport a new approach for robust configurations is followed. The notion of geometrical robustness is defined for qubit channels with power-law coupling including dipolar and van der Waals interactions. It is shown that the geometrical robustness of one-dimensional qubit arrays has two maxima and the peak positions depend on different network-environment parameters. In addition, the main peak of geometrical robustness can be also achieved by coherence-less master equation supposing dephasing noise as the line broadening of the energy levels.

In Chapter 4, switching of quantum transport is studied as another approach towards controlled quantum transport. We investigate fully symmetric three-dimensional networks of dipolar coupled qubits. It is shown that quantum energy can be trapped within such networks in terms of dark states and be manipulated via nanomechanical displacement of some part of the network as the controller. Further investigation shows that the switching characteristics persists in the presence of dephasing noise.

2

Efficient quantum transport in qubit networks

2.1 Efficient transport in one and two-dimensional dipolar coupled semi-noisy channels

2.1.1 Abstract

Transport in quantum channels is a building block of many miniaturized technologies. In dipolar channels with an irreversibly connected sink site we compare the quantum transport of different dimensional configurations and specifically show that the increase of dimension of such channels does not increase the efficiency of transport significantly. Moreover, we present patterns of optimal

configurations for robust channel design. We show that by adding one site to a one-dimensional network, the robust patterns of channel configurations in parameter space are repeated. In two-dimensional channels, the addition of one site, or a clone of n closely located sites to an arbitrary location just locally affects the optimal configurations. Since robust efficient patterns can not be easily investigated for networks with larger number of sites or high-dimensional expansions, the studied behaviours of networks of few number of sites are important for robust design of such channels.

2.1.2 Introduction

Necessary elements of complex quantum networks are efficient quantum channels transferring quantum states or energy excitations within the network [42, 43]. Qubit-based channels are implemented by different two-level physical entities like trapped ions and Rydberg atoms [44, 45], superconducting qubits [46, 47] or (synthesized) metallic nano-waveguides [1, 48–52]. The capacity of quantum channels is an asymptotic concept which is attained only in the limit of infinite uses of the resource. On the other hand, it is natural to ask what happens in settings where only some finite number of instances, in the extreme case only one instance, is available. This point of view is central to one-shot quantum information theory [53, 54], and have already found applications further afield such as area laws for entanglement in one-dimensional many-body quantum systems [55, 56].

In this paper we consider dipolar channels consisting N interacting two-level systems coupled via dipolar type interaction and irreversibly connected to an additional target qubit. This last coupling enforces some noise into the transport and we denote them as semi-noisy channels to differentiate from many other studies where each site on the network suffers noise. We numerically study such networks for optimal quantum transport in terms of varying the spatial dimension of site configurations and the robust geometrical arrangement of sites.

Regarding dimension analysis, it has been shown, for example in [57], that three-dimensional networks are $O(10^{-3})$ more efficient than one-dimensional ones. Here we will find via a random walk

optimization routine that in a wide range of network parameters, two-dimensional four-site channels are $O(10^{-2})$ more efficient than one-dimensional ones. In addition, for networks with larger number of sites for a typical set of network parameters we show that the order of such difference remains the same. From this we take that one-dimensional quantum channels are adequate, and building two-dimensional networks is demanded for specific network designs.

To build a channel, one may determine the required spatial dimensionality, and then may optimize the positions of sites. It should be considered that finding the global optimal channel configuration as the number of sites increases is computationally very costly and may not easily succeed due to the existence of many identical efficient configurations which are spread in a complex manner within their high-dimensional geometrical parameter spaces. Additionally the resulting efficient configuration may not be very robust to errors or geometrical variations. Different studies investigated robust quantum transport of general channels [18, 58–60] against different network parameters, however the exact amount of tolerable geometrical variations was not studied.

Here to provide insight on the geometrical parameter spaces of semi-noisy channels, we investigate the robust optimal configurations of few-site networks that are adequate for some quantum transport demands. We numerically find the patterns of efficient configurations in non-duplicate geometrical parameter space for channels expanded in one and two dimensions. We show that by adding one extra site to an existing one-dimensional network the optimal areas are preserved. In addition, in the more general case of two-dimensional networks, by adding a clone of n closely located sites to a three or four-site network, the optimal patterns are only locally affected by the clone. This behaviour can be considered for analyzing geometrical parameter spaces of many-site two or one dimensional networks when some sites are rather close to each other with respect to the size of the network.

2.1.3 Comparison of the efficiency of one and two-dimensional channels

We consider a network of N interacting two-level systems which initially contains one excitation on the first site. To study an irreversible transfer of the initial quantum of energy we consider a

dissipative process from the N^{th} site to a target site. In the Markovian regime, the time evolution of the energy excitation within this quantum channel is obtained by the following master equation [61]

$$\dot{\hat{\rho}} = -i[\hat{H},\hat{\rho}] + \mathscr{L}_{target}(\hat{\rho});$$
$$\mathscr{L}_{target}(\hat{\rho}) = \Gamma(2\hat{\sigma}^{\dagger}_{target}\hat{\sigma_N}\hat{\rho}\hat{\sigma_N}^{\dagger}\hat{\sigma}_{target} - \left\{\hat{\sigma_N}^{\dagger}\hat{\sigma}_{target}\hat{\sigma}^{\dagger}_{target}\hat{\sigma_N},\hat{\rho}\right\}), \tag{2.1}$$

where $H = \sum_{i=1}^{N}\varepsilon|i\rangle\langle i| + \sum_{i\neq j}J_{ij}|i\rangle\langle j|$ is the Hamiltonian of the N-site network, ε is the energy of each site, $J_{ij} = v/r_{ij}^3$ is the dipolar coupling between sites i and j located at distance r_{ij} from each other, v is the coupling strength, Γ is the dissipation rate from site N to the target, $|i\rangle$ is the quantum state of the system indicating one excitation on site i, and $\hat{\sigma_i}^{\dagger}(\hat{\sigma_i})$ is the Pauli creation (annihilation) operator applied to site i. In order to solve Eq. (2.1) we consider a Hilbert space of rank $N+1$ where the $N+1^{st}$ corresponds the target site. Converting the total density matrix of the system of rank $(N+1,N+1)$ to a vector (ρ_{vec}) of rank $((N+1)^2,1)$ in a column-wise manner, yields the linear matrix equation of $\rho_{vec} = M.\rho_{vec}(0)$ where M is a super-operator matrix of rank $((N+1)^2,(N+1)^2)$. We quantify the transport efficiency of such semi-noisy channels by the population accumulated in the target site calculated by Eq. (2.1) at a specific time i.e. $\rho_{N+1,N+1}(t)$.
Now to compare the efficiency of one and two dimensional networks we consider a four-site channel in which the position of the first and last sites are fixed on the x axis at $x_1 = -1$, and $x_4 = 1$ and the self-energies of sites are zero ($\varepsilon = 0$). Different one-dimensional networks are made up by locating the two interior sites arbitrarily on the x axis between the two fixed sites. On the other hand, the two-dimensional channel configurations are described by interior sites positioned inside a dashed square as shown in Fig. 2.1(1). Through a random walk optimization process we find the global maximum of target population for various configurations of one and two-dimensional networks for all sets of network parameters (time of measurement Γt and coupling strength Γ/v). The random walk optimization routine in a few different turns chooses about 10^2 different initial random positions for the interior sites of one and two-dimensional networks. Then for each initial

random configuration we search for a local maximum of efficiency of transport by taking 1.5×10^3 Gaussian random steps of width 10^{-3} which are adding to the position of an arbitrary interior site. Fig. 2.1(2) shows the difference between the maximum found target populations of one and two-dimensional four-site networks for the whole range of network parameters ($\Gamma t, \Gamma/v$). It can be seen that the maximum difference of the efficiency of one and two-dimensional networks which occurs in two parameter regions is of the order of 10^{-2}. The regimes of network parameters of 2D

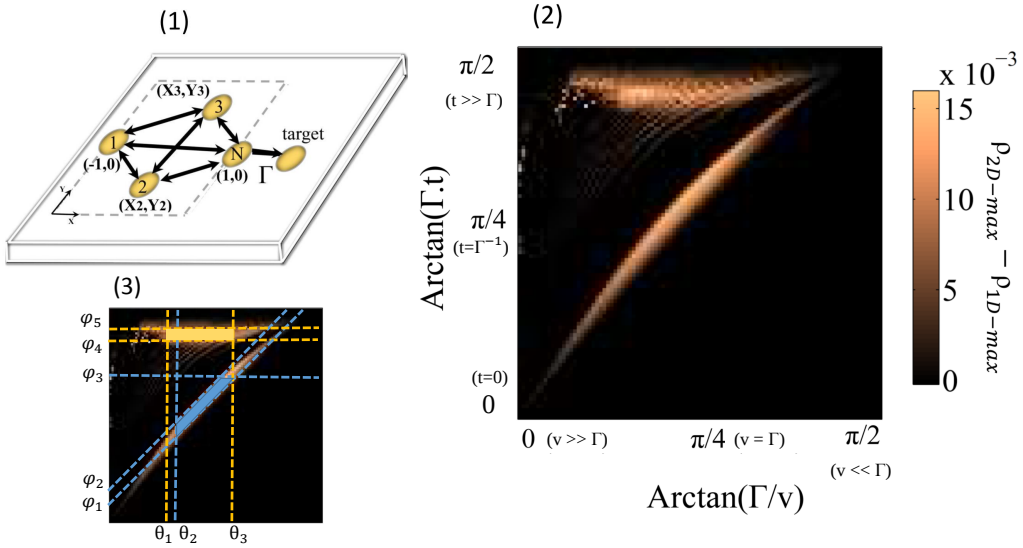

FIGURE 2.1: Here we observe that two-dimensional spatial networks can be more efficient at quantum transport than one-dimensional equivalent networks. Sub-figure (1) shows the schematic of a two-dimensional four-site network irreversibly connected to a target site. The dashed square indicates the domain of possible locations of sites 2 and 3. In sub-figure (2) the difference in transport efficiencies between one and two-dimensional networks are plotted. The one-dimensional networks are due to $Y_2 = Y_3 = 0$. The color bar shows the difference between the transport efficiency of the best configuration of one and two-dimensional networks optimized over the positions (1D and 2D), of the two interior sites in a four-site network as a function of network parameters of time of measurement and coupling strength (Γt, and Γ/v). The small difference in efficiencies indicates that to transport a quantum pure state between the first and the target sites building a one-dimensional channel is almost optimal. Sub-figure (3) highlights the two areas with 2D preferential configurations. The constraints on network parameters Γt, and Γ/v are described by the boundary values of ($\phi_1 = \pi/28, \phi_2 = \pi/14, \phi_3 = 19\pi/56, \phi_4 = 3\pi/7, \phi_5 = 13\pi/28, \theta_1 = \pi/7, \theta_2 = 5\pi/28, \theta_3 = 17\pi/56$)

preferential configurations are abstracted in Fig. 2.1(3) and described as following:

(1) The blue isosceles trapezoid: $\frac{(1-\tan\phi_1.\Gamma.t)}{(t+\tan\phi_1/\Gamma)} < v < min[\frac{(1-\Gamma.\tan\phi_2.t)}{(t+\tan\phi_2/\Gamma)}, \Gamma/\tan\theta_2]$ & $t < \tan\phi_3/\Gamma$, and

(2) The yellow rectangle: $\tan\phi_4/\Gamma < t < \tan\phi_5/\Gamma$ & $\Gamma/\tan\theta_3 < v < \Gamma/\tan\theta_1$, where t, v, and Γ are

the network parameters and $\phi_1 = \pi/28, \phi_2 = \pi/14, \phi_3 = 19\pi/56, \phi_4 = 3\pi/7, \phi_5 = 13\pi/28, \theta_1 = \pi/7, \theta_2 = 5\pi/28, \theta_3 = 17\pi/56$ as shown in Fig. 2.1(3).

Showing the corresponding 2D optimal configurations of these network parameter regimes is complicated for four site networks as the geometrical parameter space is a film. However the visualization of the comparison of 1D and 2D optimal configurations is simpler for three site networks. Fig. 2.2 shows the dimensionality preference of $N = 3$ networks with network parameters of $\Gamma/v = 1$, and $\Gamma.t = 1.4$ which are within the first region of 2D preferential configurations. It can be seen that there are two areas in 2D configurations that are about 0.05 more efficient than the 1D networks located on the x axis.

So far we investigated the effect of dimensionality on transport efficiency of four-site networks.

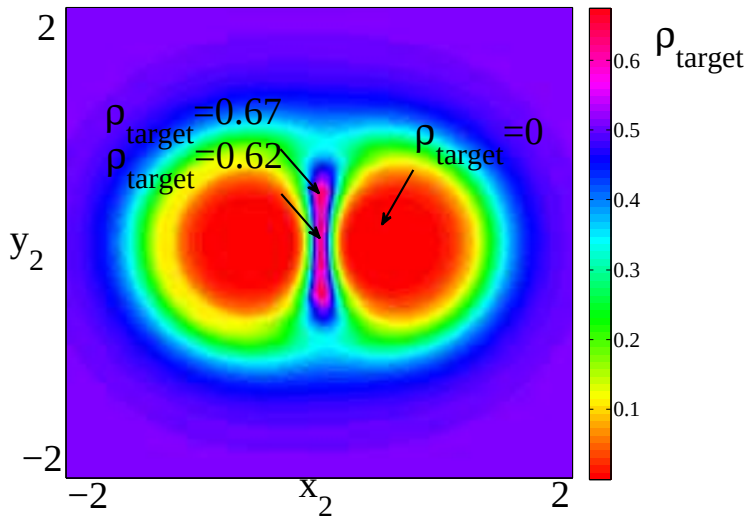

FIGURE 2.2: Here we consider a three-site semi-noisy network to compare the more efficient 2D configurations with respect to the 1D counterparts. It can be seen that for a chosen set of network parameters of $\Gamma/v = 1, \Gamma.t = 1.4$, there are two off-axis configurations that are 0.05 more efficient than the on-axis one.

To generalize our findings for networks with larger number of sites we only study one set of network parameters since the corresponding computational costs grow enormously. Table 1 shows the difference between the transport efficiencies of two and one-dimensional networks ($\delta\rho_{21}$) of four to eight-site networks with the parameters $\Gamma = 0.7, v = 1, t = 7.143$, where x_i and y_j are the coordinates of the optimal positions of the interior sites found through random walk optimization.

It can be seen from Table 1 that for the chosen set of network parameters the increase of the number of sites does not significantly increase the difference of the transport efficiencies between the two and one-dimensional networks.

N	$\delta\rho_{21}$	$\rho_{target1D-max}$	$\rho_{target2D-max}$	$x_2,...,x_{N-1}$	$(x_2,y_2),...,\ (x_{N-1},y_{N-1})$
4	0.012083	0.962096	0.974180	-0.203304, 0.284655	$(-0.2542,0.6869)$, $(0.2647,0.2482)$
5	0.004102	0.982320	0.986422	-0.069839, 0.507384, 0.274892	$(0.129424,-0.654375)$, $(0.130894,-0.085053)$, $(0.306219,-0.040707)$
6	0.005473	0.979168	0.984641	0.529870, 0.324215, 0.122069, -0.216316	$(0.473427,-0.016478)$, $(0.049347,0.236399)$, $(0.620126,-0.052786)$, $(0.302861,-0.081090)$
7	0.016030	0.965533	0.981564	-0.536002, 0.300506 , -0.638642, -0.161135, 0.563337	$(0.169785,-0.007512)$, $(0.555746,0.001822)$, $(-0.195955,0.056127)$, $(-0.439371,0.170068)$, $(0.400808,0.286340)$
8	0.014855	0.979812	0.984576	0.023681, 0.699787, -0.161214, 0.651327, 0.564224, -0.186924	$(-0.544771,0.001322)$, $(0.355224,0)$, $(-0.097140,-0.004214)$, $(-0.444345,0.002384)$, $(0.224117,-0.120531)$, $(0.530776,0.003443)$

TABLE 2.1: In this table the transport efficiencies of one and two-dimensional networks are compared with each other for larger networks of up to $N = 8$ number of sites in one case of network parameters $\Gamma = 0.7; v = 1; t = 7.143$. The optimized coordinations of the network sites of 1D and 2D networks are $(-1,x_2,...,x_{N-1},1)$, and $((-1,0,)(x_2,y_2),...,(x_{N-1},y_{N-1}),(1,0))$, with the corresponding target populations of $\rho_{target1D-max}$ and $\rho_{taregt2D-max}$. It can be seen that two-dimensional networks with $N = 4-8$ number of sites are more efficient than one-dimensional ones, however increasing the number of sites does not significantly increase this difference. Thus we expect that one-dimensional networks should be close to optimal for quantum transport for large N.

We have also studied some specific cases of semi-noisy channels in which the site distances

are in the range of $[10^{-5}, 5\times10^{-2}]$. To calculate the transport efficiencies of these networks we used *MATLAB ODE* solvers for the stiff problems and realized that the network efficiency does not depend on site distances within such small separations.

In this section we compared the transport efficiencies of four-site networks expanded in one and two dimensions within a wide range of network parameters. We found that for some choices of network parameters the two-dimensional networks are more efficient than one-dimensional ones. Moreover, the dimension comparison of the networks with larger number of sites also shows that the order of the difference of transport efficiencies of two and one-dimensional networks is 10^{-2}.

2.1.4 Efficient patterns of sites configurations in one and two-dimensional networks

Here we study the optimal geometries of one and two-dimensional networks for efficient transport. However one-dimensional networks are included in two-dimensional geometries, their individual study is important due to their simpler and more compact structure and that their efficiencies are in most cases the same as two-dimensional networks.

On-axis networks

In this section we investigate the patterns of configurations for efficient transport of one-dimensional semi-noisy channels. The positions of the first and last sites in all networks are on the x axis at $x_1 = -0.5$, $x_N = 0.5$, the relative coupling strength is $v/\Gamma = 1$, and the time of measurement is $\Gamma t = 100$ unless stated. We seek one-dimensional network configurations for efficient quantum transport to a target site which is irreversibly connected to site N. The target populations of few-site one-dimensional networks with non-duplicate configurations is shown in Fig. 2.3. According to Fig. 2.3(1) there are two efficient robust classes of four-site semi-noisy channels: (1) two interior sites located within a distance from each other i.e. the bright region near the diagonal axis of $X_2 = X_3$. The geometrical robustness of this channel or the maximum separation distance between the pair of interior sites (Z) varies so that the pair width maximum is in the center of the network, (2) interior sites located symmetrically with respect to the centre of the network i.e. the

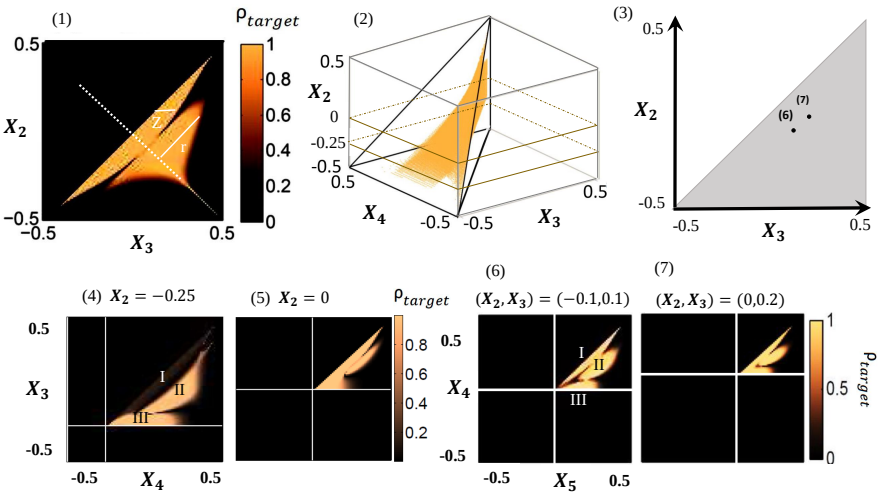

FIGURE 2.3: This figure shows the efficiency of different configurations of four-site networks as well as the main efficient configurations of five and six-site networks with parameters $v/\Gamma = 1; \Gamma.t = 100$. Sub-figure (1-3) shows the non-duplicate parameter space of one-dimensional four to six-site networks, respectively. According to part (1) there are two classes of efficient four-site networks that correspond to pair and symmetric configurations of the middle sites. Sub-figures (4,5) show two cross sections of the pyramid parameter space of Sub-figure (2). They confirm that the robust efficient configurations of five-site networks are the pair configurations of the first and last middle sites (sites 2,3 and sites 4,5, respectively) as well as symmetric positions of the last middle sites (sites 4,5). Sub-figures (6,7) show the robust patterns of efficient configurations of one-dimensional six-site networks. It can be seen that the patterns are very similar to those of five-site networks.

central triangular area in the middle part of Fig 2(1). The robustness of such channels which is the maximum deviation from the exact symmetric positions depends on the positions of the interior sites and is marked as r in Fig. 2.3(1). When the symmetrical positions of sites two and three in Fig. 2.3(1) tend to the sites one and four, respectively (along the diagonal axis of $X_2 = -X_3$), the configurations are efficient but fragile so that by any tiny perturbation of the channel configuration the transport is completely suppressed. The rest of the configurations of Fig. 2.3(1) with an empty target site trap the initial energy within the network sites not neighboring the target.

Fig. 2.3(2) shows the efficient patterns of one-dimensional five-site networks within the pyramid including unique configurations. The brown points represent network configurations with transport efficiency of %80 of that of the best configuration. Fig. 2.3(4,5) show two typical cross sections of the pyramid. As the perpendicular white lines in Fig. 2.3(4,5) are at the position of the second site, it can be confirmed that the following three classes of robust optimal configurations exist for

five-site channels: (1) area I in Fig. 2.3(5) which is a bright region near the diagonal axis: sites three and four are located within a distance from each other, (2) area II: sites three and four are in symmetric positions with respect to the center of sites two and five, and (3) area III: sites one and two are within a close distance from each other while the fourth site is around the centre.

Now we show the main region laws of one-dimensional six-site networks. The lower diagonal part of the space X_2X_3 in Fig. 2.3(3) is a schematic of a four-dimensional non-duplicate parameter space in which each point includes a lower diagonal part of space X_4X_5 indicating a unique configuration of the six-site network indexed by (x_2, x_3, x_4, x_5). The optimal patterns of lower diagonal space of X_4X_5 corresponding the marks (6) and (7) on Fig. 2.3(3) are shown in Fig. 2.3(6), and Fig. 2.3(7), respectively. The vertically crossing white lines show the position of the 3^{rd} site confirming the relation $x_i < x_{i+1}$ for non-duplicate configurations. It can be seen that the main robust classes of efficient configurations are the same as those of five-site networks. Appendix 1 provides more points and cross sections of Fig. 2.3(2,3) showing robust and fragile efficient configurations of five and six-site one-dimensional channels. Although optimizing such networks is costly, one can design few-site semi-noisy channels according to the presented robust efficient classes of configurations.

So far we discussed the patterns of efficient configurations for a typical case of network parameters $v/\Gamma = 1; \Gamma.t = 100$. Next we consider other cases of network parameters and show that the patterns of efficient configurations remain the same as that of the previous case. However the maximum efficiency or the extension of efficient areas in the parameter space change. We empirically prove this by considering nine different sets of network parameters. Fig. 2.4 show the target population of one-dimensional four-site networks in non-duplicate parameter space of X_2X_3 with various network parameters, where $(\Gamma.t)$ and Γ/V are the normalized time and the coupling strength. It can be confirmed from this figure that in different network parameters the efficient patterns of different network parameters are the same as that of the main case study, however the efficiency and the extension of some regions within the parameter space X_2X_3 vary. So it supports our hypothesis that the stated categorized efficient patterns of one-dimensional networks are the only possible ones for different network parameters.

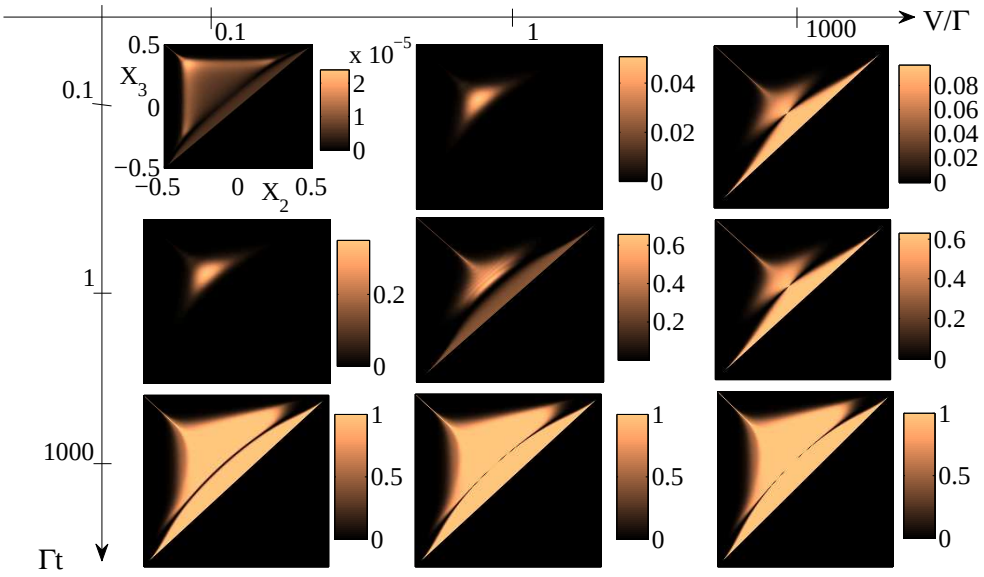

FIGURE 2.4: This figure represents the efficient configurations of one-dimensional four-site networks with nine different sets of network parameters where the first and last sites are located at $x_1 = -0.5, x_4 = 0.5$. The normalized network parameters of time $\Gamma.T$, and coupling strength V/Γ take three values of $(0.1, 1,$ and $10^3)$. It can be confirmed that the pattern of optimal configurations of almost all range of network parameters V,t are the same as the sample case of $(V/\Gamma = 1, \Gamma.t = 100)$ discussed in this section.

Off-axis networks

Now we discuss the optimal properties of the more general two-dimensional geometries. All network parameters are considered the same as those of the previous section. At first we study the complete pattern of efficient configurations of two-dimensional three site networks.

Fig. 2.5(1) shows the population of the target site of all network configurations of a two-dimensional three-site network formed by different positions of the second site (X_2, Y_2) around the first and third sites located at $(-0.5, 0)$ and $(0.5, 0)$, respectively. The patterns show that all network configurations are optimal except the ones in the dark regions around the first and third sites ($r_{1,N-1} \leq R$, $r_{N,N-1} \leq R$; regions 1 and 2, respectively), or near the circumference of a circle around the last site which crosses the first site ($r_{N,N-1} \approx r_{1N} + \delta$; region 3). Fig. 2.5(4-6) show the populations of the other sites of the network. It can be confirmed from region 1 of Fig. 2.5(1,4-6) that by tiny changes of the position of site 2 around site 1, the energy excitation rapidly oscillates between sites 1 and 2. By increasing the distance between the first two sites, the energy excitation

starts oscillating between the first and the third sites, and by a further increase the whole excitation directly tunnels through to the target site without populating other sites. In region 2, as the second

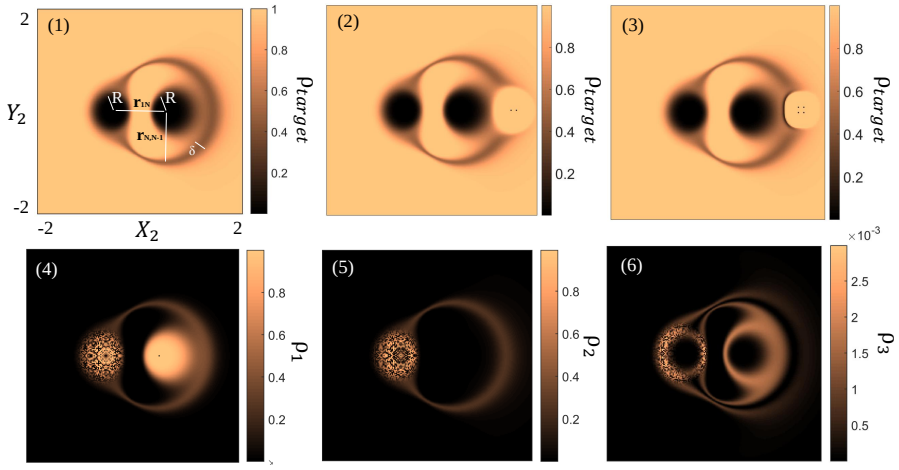

FIGURE 2.5: Efficient patterns of quantum transport in two-dimensional three-site and four-part networks with network parameters of $v/\Gamma = 1, \Gamma t = 100$. Sub-figure (1) shows the transport efficiency of all possible network configurations of two-dimensional three-site channels. Sub-figures (2,3) show the region laws of efficient transport while an extra clone of sites is added on the x axis. It indicates that adding such colony just locally changes the patterns of efficient configurations. Sub-figures (4-6) show the participation of each site in trapping the excitation for inefficient configurations.

and third sites are within a certain distance from each other the energy excitation is totally trapped on the first site and does not tunnel through to the other two highly interacting sites at the other end of the network. In region 3, the excitation is divided between the first two sites as well as the target sink. This area can be approximated as a circle around the 3rd site with the radius equal to the distance between the first and 3rd sites (r_{1N}). It can be seen from Fig. 2.5(1,4,5,6) that by locating the second site in this region the initial population will be divided within the first, second, and the target sites. The distance from the 3rd site to the first and the second sites are equal to r_{1N}, and so due the symmetric configuration of the network a standing wave is created within the first three sites. As the third and the target sites are irreversibly coupled, the population of such configurations is divided within the first two sites and the target site.

Fig . 2.6 compares the transport efficiencies of networks with different network parameters. It can

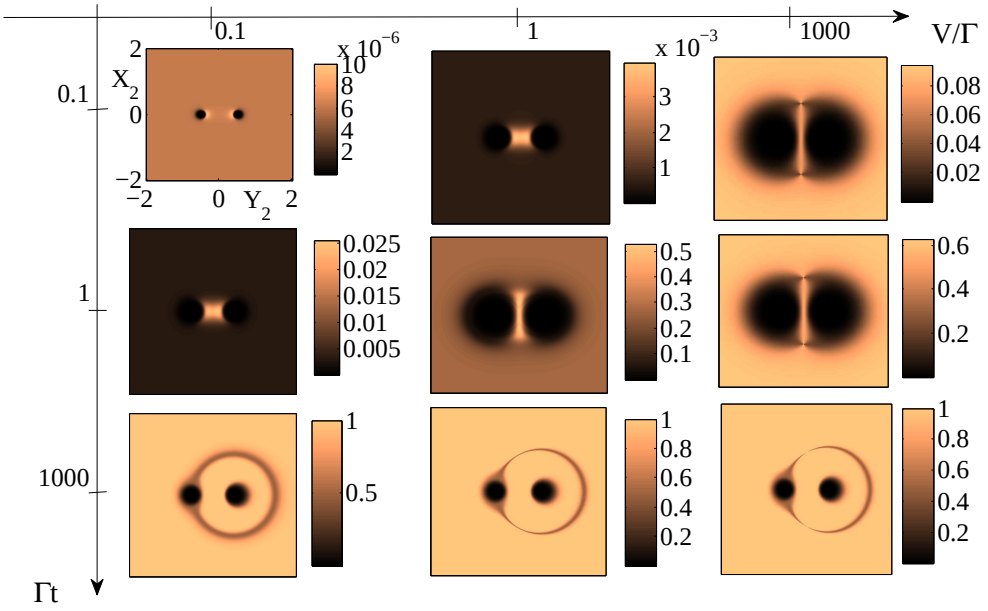

FIGURE 2.6: This figure shows the transport efficiencies of two-dimensional three-site networks with nine different amounts of network parameters. The first and the last sites are located on x axis at $x_1 = -0.5$ and $x_3 = 0.5$ where the position of the second site varies in range $X_2 = [-2,2], Y_2 = [-2,2]$. It can be seen that in lower times the efficient regions are mostly along the x axis and within the first and the last sites (i.e. $(V/\Gamma, \Gamma.t) = (0.1,1),(1,0.1)$) or along the y axis and in the center the line connecting the first and the last sites (i.e. $(V/\Gamma, \Gamma.t) = (0.1,1000),(1,1000),(1,1)$).

be seen that the area of regions 1-3 vary according to the network parameters of time and the coupling strength, however we note that these regions are the main inefficient channel configurations of two-dimensional three-site networks.

In addition, it can be confirmed from Fig. 2.5 that the initial population on site 1 can be manipulated within the four-qubit network including the target site via the mechanical control of site 2. Such irreversible control of the quantum state of semi-noisy networks may be used in irreversible quantum computing [62, 63]. Fig. 2.5(2,3) shows the effect of adding a clone of two and four sites to a three-site network leading to five and seven-site networks, respectively. It has been checked that regardless of the position of the clone, the dark patterns are just locally affected by the clone and the efficiency of the new channel increases around the clone. This is a typical pattern of robust efficient configurations in two-dimensional networks suggesting that by adding a clone of sites everywhere around but not very close to the first and last sites, the channel efficiency around the clone increases to one.

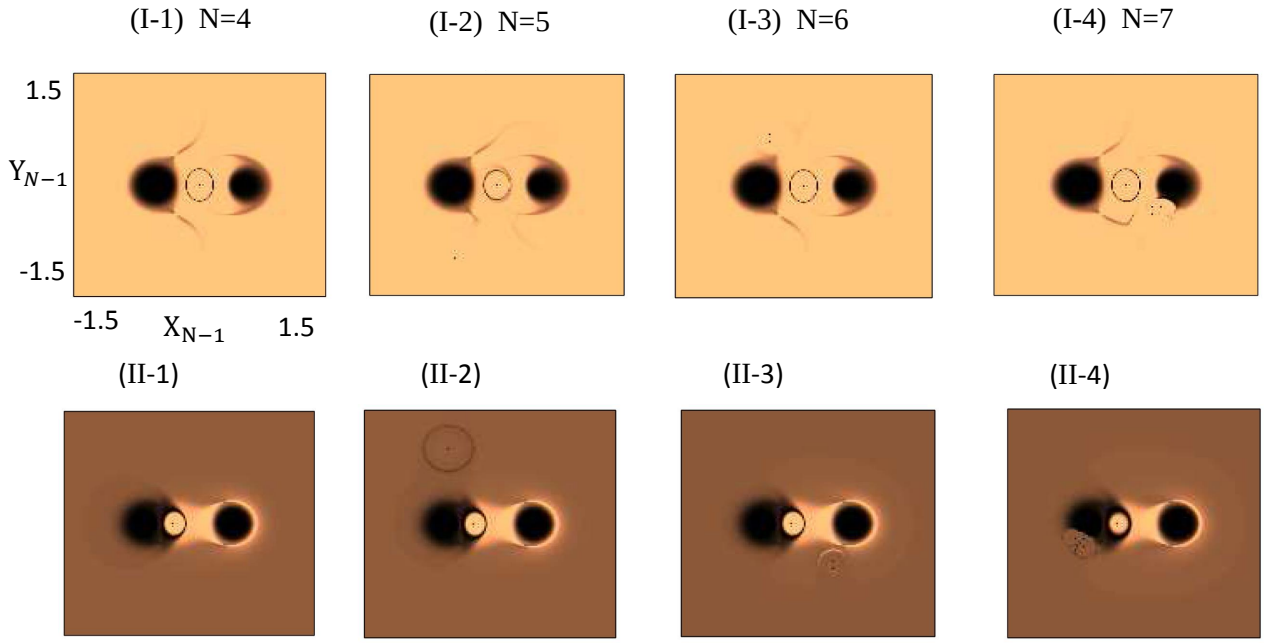

FIGURE 2.7: Patterns of efficient configurations of two-dimensional four-site and five-part networks with network parameters of $v/\Gamma = 1, \Gamma t = 100$. The first column shows two different frames of Film 1 while the second site, marked with a black point, is located on the x axis between the first and fourth sites. The 2^{nd}-4^{th} columns show the region laws of five-part networks including four sites and a clone of arbitrary number of sites located in different positions. It can be seen that the region laws of different four-site networks are just locally affected by a new colony.

In the following we investigate efficient patterns of two-dimensional four-site networks. Such efficient configurations can be found by obtaining Fig. 2.5(1) where an extra site is added in different positions around the network. Film 1 shows all corresponding efficient patterns of four-site two-dimensional networks where the second site (travelling black point) spans the upper part of a plane including the first and fourth sites. The colorbar of each frame shows the target population of networks with different positions of the third site around the first and last sites. By considering that the one and two-dimensional four-site networks have almost the same efficiency, and the fact that the non-duplicate parameter space of the two-dimensional four-site network is more complicated than that of the one-dimensional one, we just study a few cases of the efficient configurations of two-dimensional networks and do not categorize all of them.

Fig. 2.7(I-1),(II-1) show two frames of Film 1 for the cases that the second site is on the x axis

around the center, and the second site is close to the first site, respectively. It can be seen that in each case there is an efficient area around the second site which is limited by a specific radius.
The other sub-figures of Fig. 2.7 show that by adding a clone of 1-3 sites in an arbitrary position of the four-site networks of Fig. 2.7(I-1), and (II-1), the efficient patterns of configurations remain the same. This implies that adding one site or a clone of sites to two-dimensional networks will only locally change the pattern of robust efficient configurations.
It should be also noted that by changing the network parameters of time and the coupling strength the general patterns of efficient configurations of two-dimensional networks stay, however the efficiency and the extension of each pattern changes. For instance, by fixing the amount of coupling strength and increasing time, the R and δ parameters of regions 1-3 decrease.
In summary, in this section we have studied the efficient patterns of two-dimensional networks of three sites (Fig. 2.5(1)), and four sites (Film 1) for a sample choice of network parameters. We generally found that there are two main inefficient circular areas around the first and last sites that should be avoided in network designs. In addition, adding a clone of sites to the three or four-site networks provides an efficient area around the clone which only locally affects the other efficient patterns of the network within the parameter space.
At the end, we would like to interpret the results of this subsection from a different point of view. Considering the fact that there is no exact analytical solution of such semi-noisy networks, our numerical results are indicating that a pair or a clone of sites could isolate themselves within the network by means of not receiving or transporting energy to the rest of the network sites. The territory of this isolation or the radius of the clone area depends on the network parameters i.e. the measurement time and the coupling strength. Such phenomena could be explained by a simplified model with no target sink. Fig. 2.8 shows the four eigenvalues of such system with three sites at fixed positions ($x_1 = -0.5, x_3 = 0, x_4 = 0.5$) and a site spanning the x axis (x_2). The eigen-states of pair areas are stated in the boxes and they gradually convert to each other in intermediate regions through the superposition states.

It can be seen that in pair configurations the lowest energy level of the system falls off. The

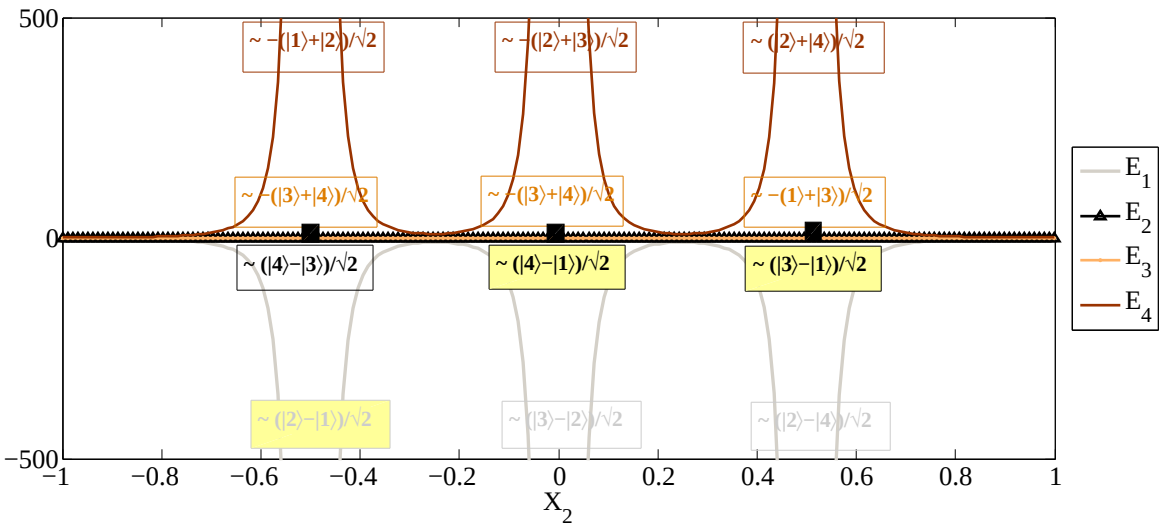

FIGURE 2.8: The graph shows the eigen-energies of four-site noise-less networks with different configurations. Three sites are located at fixed positions $x_1 = -0.5$, $x_3 = 0$, and $x_4 = 0.5$, respectively and one site (x_2) spans the x axis creating different site patterns. It can be seen that there are three energy wells around the three pair configurations of sites (1,2), (3,2), and (4,2). The approximate eigen-states of the well areas are presented in boxes of the same colors as eigen-values. As the system is initialized with one excitation on site 1, different network configurations will turn to the lowest eigen-energies with an eigen-state including $|1\rangle$ i.e. the highlighted boxes. These results confirm the inefficient areas around the first and last sites of semi-noisy networks as well as the efficient areas around a middle site.

eigen-state of the lowest energy is an anti-symmetric state of the pair sites as shown in gray boxes. By initializing the system with one excitation at first site i.e. $|\psi(0)\rangle = |1\rangle$, the state of the system approaches the lowest eigenenergy with an eigen-state including the state $|1\rangle$. In Fig. 2.8 the highlighted eigen-states in yellow correspond such systems with three different pair configurations. These eigen-states have been presented in different figures of this section. For example, Fig. 2.5 confirms that by locating site 2 near site 1 which contains one excitation, the total energy of a two-dimensional three-site network would only bounce within these two sites and cannot reach the target site. This area was previously called the inefficient region 1. By locating the second site close to the last site the system approaches the eigen-state including these pair of sites leading to a zero population of the target site (Fig. 2.5(4)). Another example is a pair configuration that does not include the first and the last sites i.e. the efficient configurations around the clones of Fig. 2.5(2,3) and Fig. 2.7((I-1)-(I-4)). In these cases the clone would hardly interact with the first

and the last sites yielding an efficient discharge of excitation from the last site to the target site. Other efficient or inefficient configurations shown in the figures of this section cannot be directly explained from the energy levels of the noise-less systems.

2.1.5 Conclusion

The transport of pure quantum states is studied in networks of two-level systems with single excitation approximation. The sites are considered dipolar coupled and only one qubit is irreversibly connected to a target site. It is numerically proved that quantum transport in one-dimensional dipolar semi-noisy channels is almost as efficient as two-dimensional ones and there is no specific dimensionality preference for designing this type of channels. We also studied the patterns of efficient configurations of such channels and showed that by adding the number of sites by one the introduced classes of efficient patterns are being repeated. We also found that by putting a clone of sites in an arbitrary location, the robust efficient patterns are locally affected by the clone. The empirical behaviours of efficient transport found can be used for robust optimal design to irreversibly transfer a pure quantum state to a neighbouring device.

2.1.6 Appendix 1

In this appendix we show more details of efficient configurations of one-dimensional five and six-site networks which may not be robust. Fig. 2.9 shows more cross sections of the essential pyramid of five-site networks in Fig. 2.3(2). It can be confirmed from Fig. 2.9(2-6) that the fragile and robust efficient configurations are as the following: (1) the first three sites (1-3) are in the vicinity of each other at one end of the network while the fourth site is not close to the fifth site, (2) the first two sites (1,2) are close to each other as well as the last two sites (4,5), while site 3 is around the center, (3) the first two interior sites (2,3) are closely located to each other but not close to the lateral sites, (4) the last two interior sites (3,4) are in symmetric positions with respect to the center of the subnetwork of sites 2-5, (5) the last two interior sites (3,4) are close to each other while site 2 is not close to the first site, and (6) all three interior sites are in the center of the network and in the vicinity of each other. Fig. 2.10 shows the detailed efficient patterns of six-site

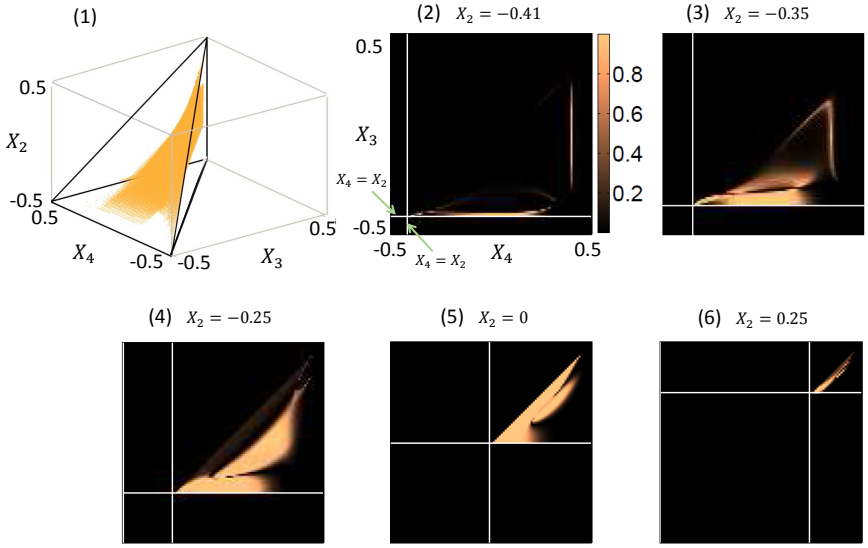

FIGURE 2.9: The target population (colorbar) of one-dimensional five-site networks with robust and fragile configurations are shown for network parameters $t\Gamma = 100, v = 1$. Sub-figure (1) shows the optimal configurations (possessing target population of more than %80 of that of the best configuration) with brown marks in the black pyramid including non-duplicate configurations. Sub-figures (2-5) show different cross sections of the pyramid when site 2 is located in five different positions while the colorbars show the target population of each unique configuration indexed by (x_3, x_4). It can be seen that the robust efficient configurations of five-site networks could be found by combining those of smaller number of networks.

channel configurations which may be fragile due to the geometrical perturbations. Fig. 2.10(I) is a schematic of a "super 2D" cross section of a four-dimensional triangle of the corresponding unique configurations i.e. the lower diagonal part of the space x_2x_3 in which each point represents a lower diagonal part of the space x_4x_5. Each black mark on the x_2x_3 space of Fig. 2.10(I) is shown in Fig. 2.10(II) where the colorbars show the target populations of each network configuration specified by the corresponding site coordinates of (x_2, x_3, x_4, x_5). The vertically crossing white lines are at the position of the 3^{rd} site and the relation $x_i < x_{i+1}$ confirms the uniqueness of the specified configurations. It can be seen in Fig. 2.10(II) that the efficient patterns of configurations of each row possessing a fixed x_2 are similar and by increasing x_3 or switching to the next column, the efficient areas are scaling down. This confirms a general rule of six-site channels that is by fixing the position of the second site in an arbitrary place, the efficient pattern of the rest of the sites is regardless of the position of the third site and only depend on the second site. According to Fig. 2.10(II) the following efficient classes can be distinguished for six-site semi-noisy channels:

(1) the pair configurations of sites 4,5 which are not close to the lateral sites of 3 and 6 (in rows 1-4: $x_2 = 0.3, 0.1, 0, -0.1$), (2) the symmetric configurations of sites 4,5 with respect to the center of the subnetwork of sites 3-6 (rows 1-4), (3) sites 3-5 are close to each other around the center (rows 1-4), (4) the 5^{th} site is in a certain distance from the 6^{th} site (rows 5,6).

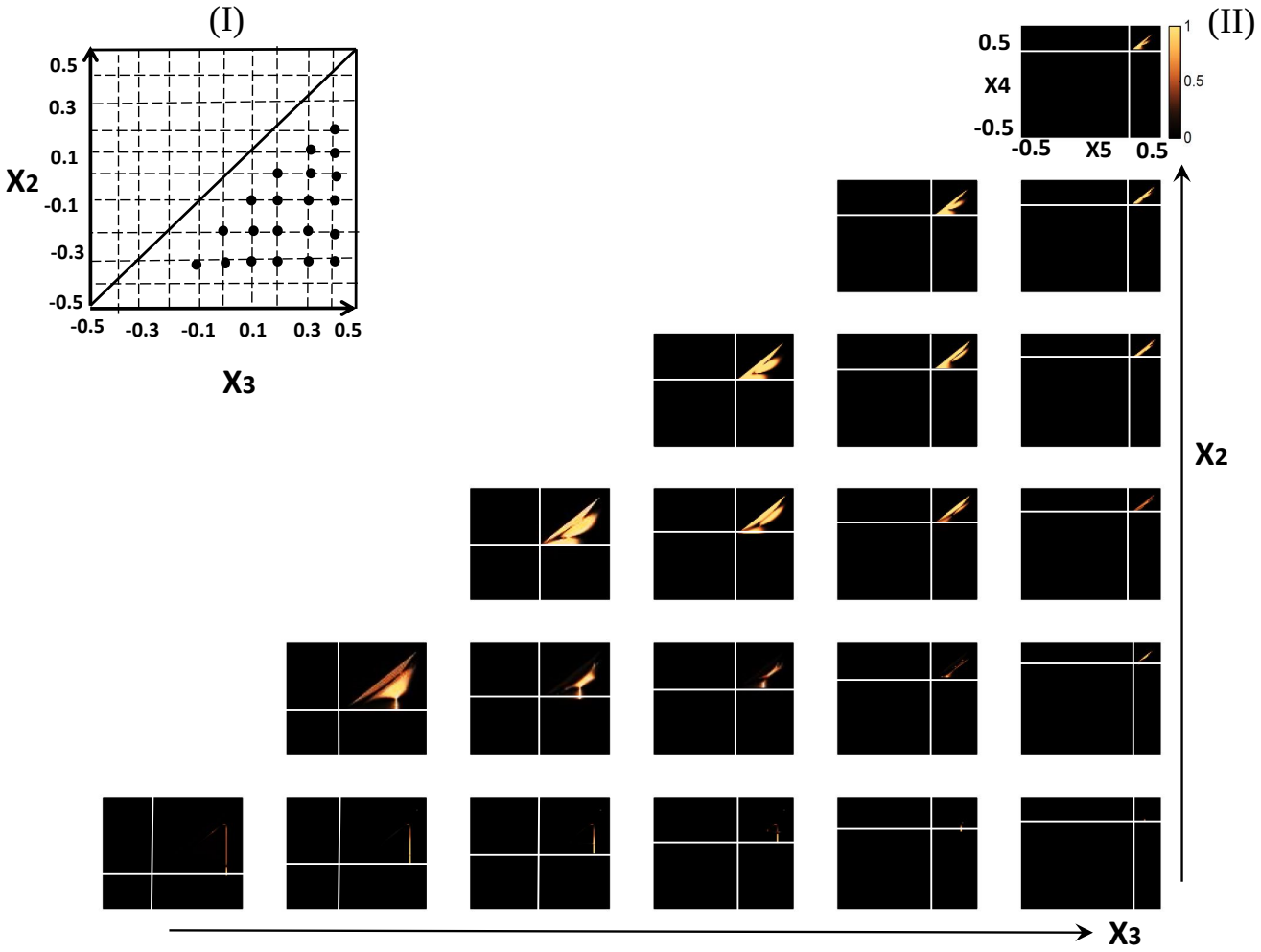

FIGURE 2.10: This figure shows the fragile and robust configurations of one-dimensional six-site networks. In subfigure (I) the lower diagonal part of the space x_2x_3 is the schematic of a "super 2D" triangle of the non-duplicate parameter space of a six-site network, where each point represents a lower diagonal part of space x_4x_5, in which each point indexes a unique configuration of a six-site network. The x_4x_5 space corresponding the black points on sub-figure (I) are shown in sub-figure (II). Since the patterns on each row are similar and by increasing x_3 the patterns are just scaling down, it can be concluded that the pattern laws of sites 3,4, and 5 only depend on the position of the second site. In general, the area laws of six-site networks are a combination of those of fewer-site networks.

2.2 Supplementary materials

2.2.1 Comparison of one and two-dimensional qubit configurations

In section 2.1.3 the spatial dimension preference of efficient network configurations has been discussed. We have shown that the transport efficiency of two-dimensional four-site networks are $O(10^{-2})$ larger than that of one-dimensional equivalent networks. Such differences in efficiencies have found for specific areas of the parameter space of coupling strength and the time of measurement shown in Fig. 2.1(2). In Appendix 1(A1) the optimal two-dimensional configurations that are more efficient than the one-dimensional ones are presented in Tables (A1-A5) which correspond to some points or specific lines of the parameter space of $\Gamma T v$ within the brown areas of Fig. 2.1(2).

2.2.2 Π-chain networks

In this part we propose an example of a new type of qubit networks extended in one and two dimensions in order to compare the transport efficiencies of such networks with different spatial dimensions. We introduce Π-chain networks consisting of a straight chain of equidistantly positioned $(N-2)$ sites displaced a perpendicular distance h (chain height) from the line connecting the first and last sites (inset of Fig. 2.11). The first site is initially populated with one energy excitation and the last site is irreversibly connected to a target site. Now by studying the Π-chain networks we can compare the transport efficiencies of one and two dimensional networks i.e. ON axis (straight chain) and OFF axis Π-chain. Fig. 2.11 shows the target population of N-site Π-chains with network parameters of $v/\Gamma = 1, \Gamma t = 1$. By increasing the chain height h the target population increases to a maximum. As the maximum efficiency is due to $h > 0$ it can confirmed that the transport efficiency of two dimensional Π-chain networks exceeds that of one-dimensional networks. With further increase of the chain height the transport efficiency decreases (for particular chain length) to zero indicating that the initial excitation is trapped within the chain. By further increasing the chain height, the target population gradually tends to that of a two-site network ($\rho_{target} \approx 0.3$) where the chain is no longer effective in the transport. So by adjusting the height of

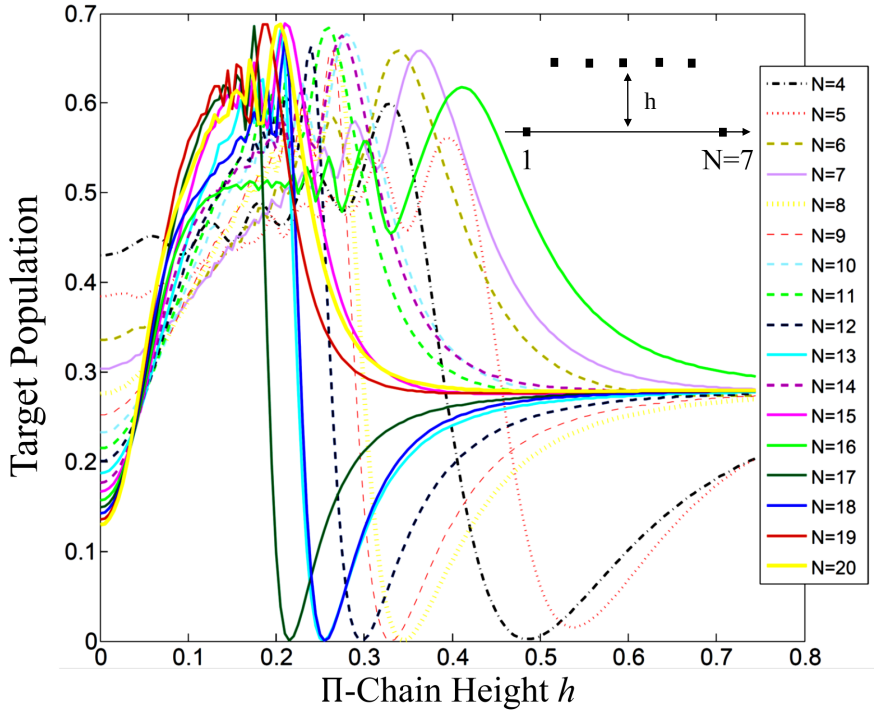

FIGURE 2.11: This figure shows the transport efficiency of different Π-chain networks as a function of chain height. The target populations display complex oscillations with certain length Π-chains yielding trapping (zero target population), and maximal (target population>0.6) excitation transfer. In the case of many particle Π-chains the optimal configuration is not when $h=0$ i.e. when the dimension of the Π-chain exceeds one.

such networks one can control the transport of the initial excitation to the target site from the zero amount to a maximum amount in terms of switching.

In addition, it can be confirmed from Fig. 2.11 that by increasing the number of sites, the target population of one-dimensional chains (i.e. $h=0$), decreases. However for non-zero chain heights ($h>0$) the efficiency fluctuates in some cases. We conclude that in such networks, by increasing the chain height, or equivalently increasing the network dimension from one to two, the optimal transport efficiency increases.

2.2.3 Clone configurations of qubit networks

In this section we discuss the transport efficiency of qubit networks with large coupling strengths ($>10^5$). In dipolar qubit networks such large couplings are due to the site distances of less than

0.01 which indicates that some qubits are located close to each other as a clone. To solve the corresponding system of differential equations we used $ode15s$ function of $MATLAB$ which efficiently solve such stiff problems.

Tables 7-9 of Appendix 1(A2) show the transport efficiencies of networks including a pair of sites separated by $10^{-3} < O(\delta x_{min}) < 10^{-15}$ for different choices of network parameters. It can be seen that the transport efficiencies of such networks are identical up to about 9-10 decimal digits. It it also found that the network efficiency of one-dimensional four-site networks including an interior pair of sites is equal to that of a two-site network. So the target population of such networks does not depend on the location of the interior pair of sites but the network parameters. So the pair of sites do not participate in the excitation transfer within the network.

It has been also checked that a clone of arbitrary number of sites do not participate in the excitation transfer and the corresponding target population is equal to that of a two-site n-dimensional network. Moreover, by putting more clones in different points or even changing the site energies of different clones the system behaves the same as the clones do not participate in quantum transport process.

By approaching the clones to the two lateral fixed sites of the networks the target population decreases to zero. In these cases, each of the first or last sites becomes a part of the clones and so does not participate in the excitation transfer. As the whole excitation is initially in the first site and the last site is the only site connected to the target sink, the lack of participation of each of these two sites in quantum transport leads to zero population transfer.

2.3 Discussions and comments

The problem introduced in section 2.1.3 was proposed by Professor Martin Plenio, my supervisor in Ulm University, who wrote the random walk optimization code and found an increase of $O(10^{-3})$ in the transport efficiency of four-site networks transferring from the first dimensional to the second one. I used tips suggested by him for searching the parameter space and could increase the difference of efficiencies to $O(0.01)$. By parallel running of the code on a cluster in Ulm I showed that the maximum difference does not exceed $O(0.01)$. Moreover, to find the rules governing the optimal positions of the network sites I suggested and developed the studies of sections 2.1.4 and 2.2. The idea of Π-chain networks in section 2.2.2 was proposed by Professor Jason Twamley, my supervisor in Macquarie University, to whom I am thankful for useful discussions regarding the preparation of this chapter. This work was funded by the ARC Centre of Excellence in Engineered Quantum Systems, ARC Project No. CE110001013, and the Alexander von Humboldt Foundation.

3

Geometrical robustness of qubit networks

3.1 Robustness of optimal transport in one dimensional particle quantum networks

3.1.1 Abstract

We study the robustness of quantum transport in four site 1D particle quantum networks irreversibly connected to a target site in the presence of environmental dephasing noise. Under conditions of Markovian decoherence we define a quantity - which we denote as geometrical robustness

- to quantify the robustness of transport with regard to the geometrical arrangement of the spin network. We examine the behaviour of this geometrical robustness for both nearest and non-nearest site interactions and show that for some values of dephasing noise and other network parameters the robustness undergoes revivals ie. the robustness periodically increase with dephasing. In addition, we find that for high amounts of dephasing noise, the pattern of optimal network configurations changes noticeably from central symmetric configurations to laterally gathered ones, and we show that this change of pattern seems to occur for any number of network sites in the 1D chain.

3.1.2 Introduction

Quantum transport is central to quantum information and quantum computation and will be a required feature among many quantum devices [15, 16, 64]. Quantum transport is widely studied in networks with the aim of achieving flexible transport of different types of excitations along one dimensional space (1D) channels [1, 2, 65]. While the effects of system environment or fabrication disorders are inevitable, achieving high efficiency robust quantum transport in the face of such deleterious effects is the topic of this work.

The robustness of various quantum networks have been studied against different environmental perturbations, inter-site interactions, and the length of 1D networks. Several studies [18, 57–60, 66] have investigated the robustness of spin chains against static random imperfections of spin-couplings. They have quantified the robustness as the average of the transfer fidelity. In general, it is found that in quasi-Markovian regimes the transfer dynamics is rather robust while in non-Markovian regimes the dynamics is more sensitive to the static imperfections [59]. In noise-assisted transfer studies the robustness is usually quantified as the population of the target site (or sink) of the network. Studies show that the robustness of transport quantified in this way can be increased in the presence of environmental dephasing noise [26, 67–72]. In addition, it has been also checked that the fundamental mechanisms underpinning dephasing assisted transport are robust against different noise models [67].

So far transport robustness has been defined for networks with fixed couplings against small coupling perturbations, or environmental noise. However distance-dependent couplings in nano-networks, which can be highly sensitive to fabrication imperfections, may lead to variations in these coupling strengths and this can generally alter the transport efficiency. Thus, in such geometrical networks, it is vital to quantise the robustness geometrically. We introduce a geometrical measure of transport robustness (geo-robustness) as the percentage of spatial network configurations which can achieve a transport efficiency better than %80 of the optimal configuration at a standard reference evolution time. We will see that one can reach the optimal transport robustness by engineering a variety of system-environment parameters e.g. coupling strength, length of the network, evolution time, and dephasing noise rate. In addition, the dependence of the geo-robustness on the type of inter-site coupling (short range/nearest neighbor vs. long range), will be examined. By studying in detail the geo-robustness in a four site model with a target sink at one end we find curious revivals in the geo-robustness which seem to be fairly independent of the detailed model. We find that these revival features do not vary much as one considers longer 1D networks and we conjecture that these revivals may be a generic feature for any 1D network. In addition, through a specific example of network parameters we show that such revivals can also happen in coherence-less systems.

3.1.3 Modeling

In this section we analyze 1D excitation energy transfer in spin networks with one excitation. The system consists of N-sites with zero self-energies ($\varepsilon = 0$) located along one spatial dimension. The sites $i = 1,...,N$ interact via tunnel coupling with each other at the rates J_{ij}. We consider two types of network interactions: one in which all possible pairs of sites interact (we denote as type 1), and it is depicted in Fig. 3.1, and nearest-sites interaction (we denote as type 2) in which $J_{ij-type2} = J_{ij-type1}; i = j \pm 1$, $J_{ij-type2} = 0; i \neq j \pm 1$. The network is located in a homogeneous noisy environment so that all sites experience dephasing noise at rate γ. The last site (N) is connected to an additional target site or sink through an irreversible process at rate Γ. We consider

an initial excitation on the first site ($i = 1$) of the network at $t = 0$ and study the transport of this excitation through the network to the sink site. The Hamiltonian of the system can be written as:

$$H_{sys} = \sum_{i,j=1}^{N} J_{ij}\hat{\sigma}_i^{\dagger}\hat{\sigma}_j; \quad J_{ij} = v(1-\delta_{ij})/\parallel L(\mathbf{r}_i - \mathbf{r}_j)\parallel^{\alpha} + \delta_{ij}\omega_i, \tag{3.1}$$

where v is the coupling constant, δ_{ij} is the Kronecker delta function, $L\vec{r}_i$ is the position of site i, α is a constant which describes the type of power-law coupling between the sites, ω_i is the energy of site i, and $\hat{\sigma}_i^{\dagger}(\hat{\sigma}_i)$ is the creation (annihilation) operator of site i. The time evolution of the system is described via the master equation with the Lindblad operators of environmental dephasing noise and dissipative noise to the target site as [61]:

$$\begin{aligned}
&\dot{\hat{\rho}} = -i[\hat{H}_{sys}, \hat{\rho}] + \mathscr{L}_{deph}(\hat{\rho}) + \mathscr{L}_{diss}(\hat{\rho});\\
&\mathscr{L}_{deph}(\hat{\rho}) = \gamma\sum_{i=1}^{N}(2\hat{\sigma_i}^{\dagger}\hat{\sigma}_i\hat{\rho}\hat{\sigma_i}^{\dagger}\hat{\sigma}_i - \left\{\hat{\sigma_i}^{\dagger}\hat{\sigma}_i, \hat{\rho}\right\}),\\
&\mathscr{L}_{diss}(\hat{\rho}) = \Gamma(2\hat{\sigma}_{target}^{\dagger}\hat{\sigma_N}\hat{\rho}\hat{\sigma_N}^{\dagger}\hat{\sigma}_{target} - \left\{\hat{\sigma_N}^{\dagger}\hat{\sigma}_{target}\hat{\sigma}_{target}^{\dagger}\hat{\sigma_N}, \hat{\rho}\right\}),
\end{aligned} \tag{3.2}$$

where $\hbar$ is set to be unity, $\hat{\rho}$ is the density matrix of the system and environment, γ is the dephasing noise rate to the environment and Γ is the rate of irreversible energy transfer from the last site to the target site. In the next section, we study the excitation energy transfer through this 1D network. We numerically calculate the excitation transferred to the target and determine which configurations are most efficient for this transport at a specific time t. We investigate the measure of the class of efficient 1D configurations in comparison with all possible geometric configurations by defining the quantity which we denote as the "geometric robustness" of transport. Then we study how this geo-robustness is against variations of dephasing noise rate, coupling strengths, evolution time, and the number of sites.

3.1.4 Results

Robustness of transport for all-sites and nearest-sites interaction

To be concrete we choose to study four site networks in which the location of sites on the x axis are as $x_1 = -0.5, x_2, x_3, x_4 = 0.5$, where the spacial positions (x_2, x_3) can vary within the region $x_{2,3} \in (-0.5, 0.5)$. We assume a physically realistic interaction and take that sites interact as parallel dipoles $J_{ij} = v(1-\delta_{ij})/x_{ij}^3$, where $v = VL^{-3}$ quantifies the strength of the coupling, V is a constant, L is the size of the network $L = |x_N - x_1|$, and $x_{ij} = |x_i - x_j|$ is the relative distance between the sites i and j. We normalise the time, coupling strength and dephasing noise in units of Γ and consider $\Gamma t = 100$, $VL^{-3}/\Gamma = 1$, and $\gamma/\Gamma = 0$. For the rest of the study we restrict ourselves to four sites and the dipolar form of the coupling unless otherwise stated. Solving the master equation (3.2) numerically as discussed in section 2, in Fig. 3.1 we show the population of the target for all network configurations of the parameter space (x_2, x_3) for both interactions of types 1 and 2 in graphs (a) and (b), respectively. Graph (a) shows that the efficient configurations of all-site interacting systems are those in which the middle sites are symmetrically located in the network but rather far from the lateral sites. In addition, the networks with middle sites close to each other but not very close to the lateral sites are as efficient as symmetric networks. There is also a zero excitation transfer due to configurations in which the middle sites are separated from each other by a forbidden distance (border line of the spindle-form region), that decreases by moving the middle sites to the first or last sites. In part (b), it is shown that the symmetric configurations of nearest-sites interacting networks are efficient however joint configurations of middle sites (black region around the diagonal line) trap the initial excitation in the first site. It has been checked that in this case and also in the case of the forbidden distance configurations of type 1, the trapped excitation remains on the first site. In all other trapping configurations of types 1 and 2 (spindle black regions), the excitation oscillates within the first three sites and the fourth site is isolated and very little excitation makes it to the target sink.

In the literature on quantum transport the robustness of networks has been studied against random

perturbations in coupling strength [59]. Here we intend to show that even for large coupling disturbances, or equivalently significant movements of sites, the transport can be robust. We define the geometrical robustness (μ) of optimal transport at a specific time as follows: the percentage of configurations that yields a sink population better than %80 of the optimal geometric configuration at a pre-set evolution time. To visualize this, we refer to Fig. 3.1 and consider the ratio of the white and yellow area to the area of the whole parameter space of (x_2, x_3) as a measure of our robustness (μ). Numerically we discretize the (x_2, x_3) parameter space to compute this measure. In addition, as the sites are identical the fundamentally distinct configurations are those in the upper or lower diagonal part of Fig. 3.1.

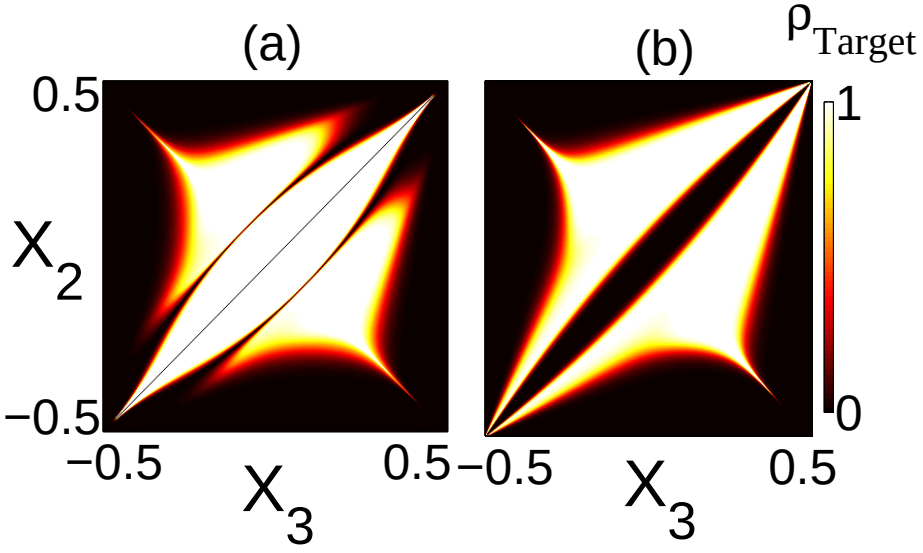

FIGURE 3.1: (Color online) This figure shows the excitation transfer to the target for all configurations of four site networks in graph (a) (type 1) and graph (b) (type 2). The sites are realized to be at ($x_1 = -0.5$, x_2, x_3, $x_4 = 0.5$), respectively. Network parameters are $\Gamma t = 100$, $VL^{-3}/\Gamma = 1$, and $\gamma = 0$. The color bar shows the population of excitation accumulated in the target at time t. In both types (a) and (b), the symmetric positions of middle sites can efficiently transfer the initial excitation to the target (bright regions); however joint configurations of middle sites are only efficient for interaction type 1. In all dark regions the fourth site of the network is isolated so that the efficiency of the excitation transfer is very small.

Variation of robustness with dephasing noise

In the above example in Fig. 3.1, we did not consider any dephasing and set $\gamma = 0$. More generally, we can consider how this robustness depends on dephasing noise, and evaluate the variation of

robustness of optimal transport (μ) against γ. Fig. 3.2 (a) shows this variation for interaction types 1 and 2 while the network parameters are $VL^{-3}/\Gamma = 1$, and $\Gamma t = 100$. Surprisingly we observe that there are two main peaks of robustness for both interaction types. Along the upward trend of the first peak, an increase in the dephasing noise results in an increase in μ. To understand this trend one may note that different network configuration (x_2, x_3), represents a distinct 1D quantum path (or a set of quantum steps along the 1D network), of excitation from the first site ($i = 1$) to the target. So as dephasing increases it seems that the density of available transport paths also increases and some of the trapping configurations involving the first three sites are circumvented. Dephasing noise breaks the symmetry of the dark states which allows new transport pathways to open up. Any oscillation of the position of the interior network sites or equivalently, more environmental dephasing noise, disturbs the energy levels of the system and the previous trapping eigenstates no longer exist. Thus by increasing dephasing the number of efficient quantum paths increases. For larger dephasing noise, the robustness reaches a maximum and starts to decrease along the downward trend off the main first peak. Due to quantum Zeno effects (or equivalently line broadening [26]), the increased dephasing noise of the excitation remains in the network and cannot transit to the target site. In the presence of dephasing noise, one can check that the initial excitation in a trapping configuration does not oscillate within the network but rather exponentially decays from the first site, and accumulates equally between the first three sites. In graph (a) there is an extra sub-peak within the first peak of interaction type 1 which is the only significant difference of robustness between the two interaction types. It has been checked that within this sub-peak of type 1 the efficient joint configurations depicted in Fig. 3.1 (a) disappear gradually with increasing dephasing. As this class of efficient paths does not exist for type 2 we expect different behaviours of robustness for these two types of coupling. Fig. 3.2 (b) depicts the pattern of reviving efficient configurations throughout the second peak of μ. We observe that in this regime of dephasing the peak of robustness is due to the spread of "good" configurations from the centric-symmetric geometries in the (x_2, x_3) parameter space to the marginal positions. Therefore, the environmental dephasing noise has a significant effect on the network optimal patterns and at

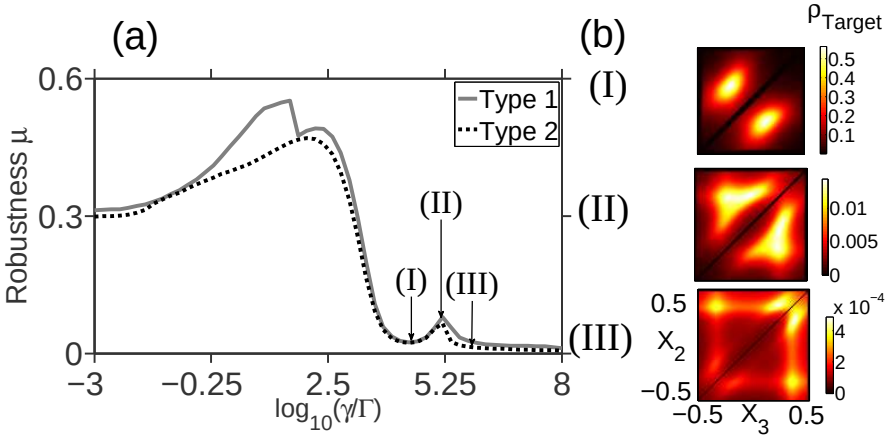

FIGURE 3.2: (Color online) Graph (a) shows the robustness μ against the logarithm of normalized dephasing noise $Log_{10}(\gamma/\Gamma)$ for interaction types 1 and 2, while network parameters are $VL^{-3}/\Gamma = 1$ and $\Gamma.T = 100$. The upward trend of the first peak for both interaction types is due to the symmetry breaking of trapping configurations, and the downward slope is due to a kind of quantum Zeno effect. Graph (b) shows the efficient configurations of type 1 networks for three different dephasing noise levels during the second peak of μ. According to these the second peak is due to the change of optimal configurations or stable energy levels of the system. The main difference of the behaviour of robustness in types 1 and 2 interactions is within the first peak (the additional sub-peak of type 1) due to the different patterns of efficient configurations shown in Fig. 3.1. During this sub-peak the joint configurations of type 1 gradually disappear with increasing dephasing.

the value of the top of the second peak acts as the order parameter to transit between different geometrical arrangements of efficient configurations.

Variation of robustness with network couplings

Now we study the effect of network coupling strength on the robustness oscillations we noted above. Fig. 3.3 (a) shows the variation of robustness (μ) for the more complicated interaction of type 1 for various normalised coupling strengths (VL^{-3}/Γ) and dephasing noise (γ/Γ), while $\Gamma t = 100$. In order to change the strength of the coupling between the sites, one can change V or the network size L (the latter is factored out from the distance between network sites so that inter-site distances would vary as $dx < x_{ij} < 1$, where dx is the discretization length of the networks which is considered 0.006. The distinct border line between the yellow and black regions depicted in Fig. 3.3 (a) is the position of the first peak of robustness (μ) shown in Fig. 3.2 (a). Empirically one observes that the maximal value of robustness is located at $VL^{-3}/\sqrt{\gamma\Gamma} \simeq 0.0412$,

and the robustness is highly plateaued with a rapid fall off in the regime of $VL^{-3}/\sqrt{\gamma\Gamma} \gtrsim 0.0412$. In other words, for a given set of network parameters the first peak of robustness represents the dephasing tolerance of the system. By increasing the depahsing after the tolerance amount the transport efficiency of many optimal configurations suppress resulting a sharp reduce of robustness. Fig. 3.3(a) shows that by increasing the coupling strength the position of the first peak shifts forward indicating that the dephasing tolerance is more in networks with stronger couplings.

Above we considered the dependence of μ on $J_{ij} = v(1-\delta_{ij})/(Lx_{ij})^3$ (a dipole-dipole interaction).

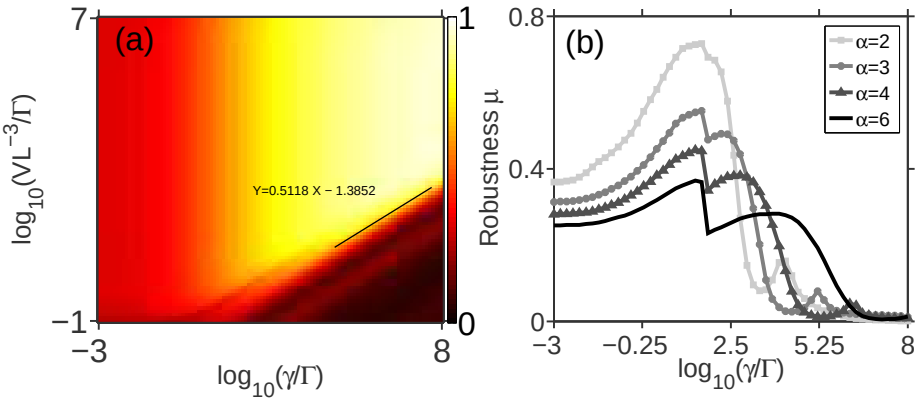

FIGURE 3.3: (Color online) Graph (a) shows how the robustness μ is influenced by the strength of tunnel coupling VL^{-3}/Γ and dephasings noise γ/Γ, while $\Gamma t = 100$. According to the sharp linear border the high values of robustness are in the regime of $VL^{-3}/\sqrt{\gamma\Gamma} \gtrsim 0.0412$, and the low values (starting from the first peak of Fig. 3.2 (a)) are in the complementary region of $VL^{-3}/\sqrt{\gamma\Gamma} \lesssim 0.0412$. The high value regime of robustness which includes symmetric configurations are growing by increasing dephasing. The position of the main peak of robustness is around $VL^{-3}/\sqrt{\gamma\Gamma} \simeq 0.0412$. Graph (b) shows the dependency of robustness on coupling rates ($J = V/(Lr_{ij})^{\alpha}$) by changing α possibly represent different physical implementations. It seems that increasing α shifts the position of the second peak to larger γ/Γ. Moreover, α does not change the position of the first sub-peak and so efficient pair levels of middle sites are not affected by the model of physical tunnel coupling.

Now we consider a more general form for these tunnel couplings to be $J_{ij} = v(1-\delta_{ij})/(Lx_{ij})^{\alpha}$. In the ion trap implementation of the network (in the adiabatic regime), one can adjust the coupling rates through a changing α experimentally [73]. Fig. 3.3 (b) shows the dependency of the oscillation of μ on the specific model for the physical tunnel couplings. Curiously we find the similar patterns of robustness as shown in Fig. 3.3(b) for interaction type 2, by focusing on the second sub-peak of Fig. 3.2(a).

In general, it can be observed from Fig. 3.3(b) that the increase of α or equivalently the decrease of J_{ij} would increase or decrease the robustness according to the value of dephasing rate. This behaviour is confirmed by Fig. 3.3(a) as well. In addition, the increase of α drives the position of the second sub-peak which correspond the symmetric configurations forward down and lowers the position of the first sub-peak corresponding the joint configurations. This indicates that the symmetric configurations of networks with van der Waals interaction have a larger depahsing tolerance than that of a dipolar interacting network; however the overall amounts of robustness is less for van der Waals interacting systems. On the other hand, the pair configurations of different power-law interacting networks have the same depahsing tolerance, although the robustness is larger for networks with stronger couplings like for $\alpha = 2$.

Variation of robustness with time

The next important parameter that we discuss is time. In Fig. 3.4 the dependence of the robustness (μ) on time and depahsing noise is shown while $VL^{-3}/\Gamma = 1$. It is clear that the position of the peaks introduced in Fig. 3.2 (a) move forward linearly with increasing time and dephasing i.e. the position of the peak is a linear function of Γt depicted as a black line on Fig. 3.4. Above this line ($\Gamma^2 T/\gamma \gtrsim 0.0463$) robustness is high and for the complement region of network parameters ($\Gamma^2 T/\gamma \lesssim 0.0463$) robustness drops to a low value. It can be also confirmed from Fig. 3.4 that for longer time shots, the four site system can tolerate a larger dephasing noise before most network configurations shrink the transport and reduce the robustness. In addition, Fig. 3.4 indicates the absence of any permanent trapping state and at the infinite time limit the robustness of all such networks would be 1; however for some dephasing regimes to reach the unit robustness one should wait more than $10^7\Gamma$. It can be inferred from Fig. 3.4 that for a given set of network parameters one can find the appropriate time scale by which the geo-robustness of the system is optimal. On the other hand, it should be also noted that even in very large time shots, it is always possible to disable the transport of all configurations by an accordingly large dephasing noise.

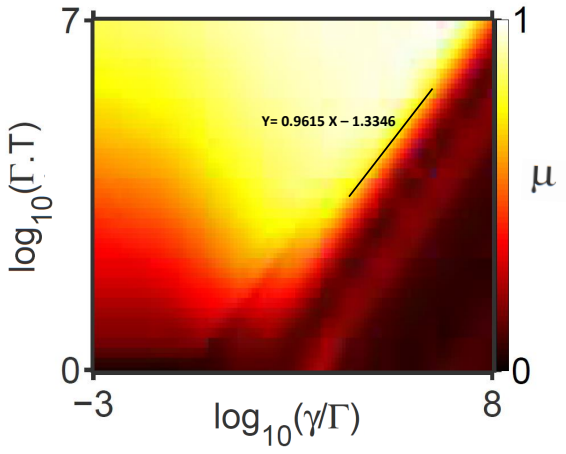

FIGURE 3.4: (Color online) The figure shows how robustness μ is influenced by Γt for different dephasing noise rates (γ/Γ), while $VL^{-3}/\Gamma = 1$. It is shown that by increasing time both peaks shift linearly forward. In addition, in the range of $\Gamma^2 T/\gamma \gtrsim 0.0463$ robustness during the first peak has large values.

Network extension

In the following we study the network extension effect on μ by adding more sites to the chain. Fig. 3.5 (a) shows the variation of robustness against dephasing noise for different numbers of network sites for network parameters $VL^{-3}/\Gamma = 1$, and $\Gamma t = 100$. It can be seen that by increasing dephasing noise, the positions of both peaks move forward and the heights decrease. In part (b) the efficient configurations of three, four , and five sites networks have been shown for different dephasing noises within the fundamental regions described as follow: The line of $x_2 = -0.5 : 0.5$ for $N = 3$, the lower diagonal part of space parameter (x_2, x_3) for $N = 4$, and the black triangular pyramid of the parameter space (x_2, x_3, x_4). For dephasing noise of $\gamma/\Gamma = 10^2$, the fundamental optimal region of three sites networks is the black line in the first column of Fig. 3.5 (b). For $N = 4$, the fundamental optimal region is the white triangular shape, and for $N = 5$ it would be the red triangular pyramid shape. When dephasing noise is $\gamma/\Gamma = 10^4$, the optimal region for $N = 3$ is a smaller black line, in four sites networks $(N = 4)$ it is approximately an ellipse, and for $N = 5$, it becomes an ellipsoid. In higher values of dephasing $(\gamma/\Gamma = 10^6)$, the optimal region for $N = 3$ is a smaller line, for $N = 4$ is two ellipses and for $N = 5$ is three ellipsoids. So it could be confirmed that by increasing the dephasing noise from $\gamma/\Gamma = 10^2$ to 10^6, the pattern

of efficient configurations in the parameter space for any number of network sites, varies from central-symmetric regions to marginal ones. It could be also predicted from the last row of Fig. 3.5 (b) that the number of robust optimal regions in high dephasing noise range ($\gamma/\Gamma = 10^6$) for N sites networks is $N-2$. In general, Fig. 3.5 (b) shows that the pattern of the variation of geo-robustness is invariant to scaling of such networks since by adding the number of the sites, the dimensions of the fundamental region and the optimal region increases. In addition, the behaviour of optimal configurations for any arbitrary number of sites in the considered dephasing noise regimes could be estimated according to Fig. 3.5(b), however the direct calculation of robustness or the optimal configurations for arbitrary larger number of sites would be very time consuming. In general, for large number of N network sites for intermediate values of dephasing noise ($\gamma/\Gamma = 10^2$ to 10^4), all central symmetric configurations in the parameter space are optimal, while in the larger regime of dephasing noise ($\gamma/\Gamma = 10^6$), $N-2$ robust regions exist in the corresponding $(N-2)$-dimensional parameter space.

The presence of entanglement

In this section we show the presence of entanglement in one dimentional four site networks. We calculate the logarithmic negativity measure of entanglement [74, 75], using a chosen bipartite split of network, e.g. the first site v.s. all other sites including the target/sink. For a 4-site chain and one target/sink, Fig. 3.6 (a), shows the amount of entanglement for all possible network couplings in (x_2, x_3) parameter space when $\gamma/\Gamma = 0, \Gamma t = 100, VL^{-3}/\Gamma = 1$. By comparing Fig. 3.1(a) and Fig. 3.6(a) one can see that in the high transport network configurations introduced in Fig. 3.1(a), the logarithmic negativity for the chosen bitartie split almost vanishes. This may be expected as there will be little occupation left in site 1 when the transport is efficient. However some entanglement exists for trapping configurations. The scattered dark points in Fig. 3.6 (a) shows the fast oscillations of entanglement due to changes in network couplings, which has been observed before (though with respect to time) [26]. From this one can deduce that inefficient transfer configurations posses trapped states and exhibit quantum entanglement - a purely quantum mechanical

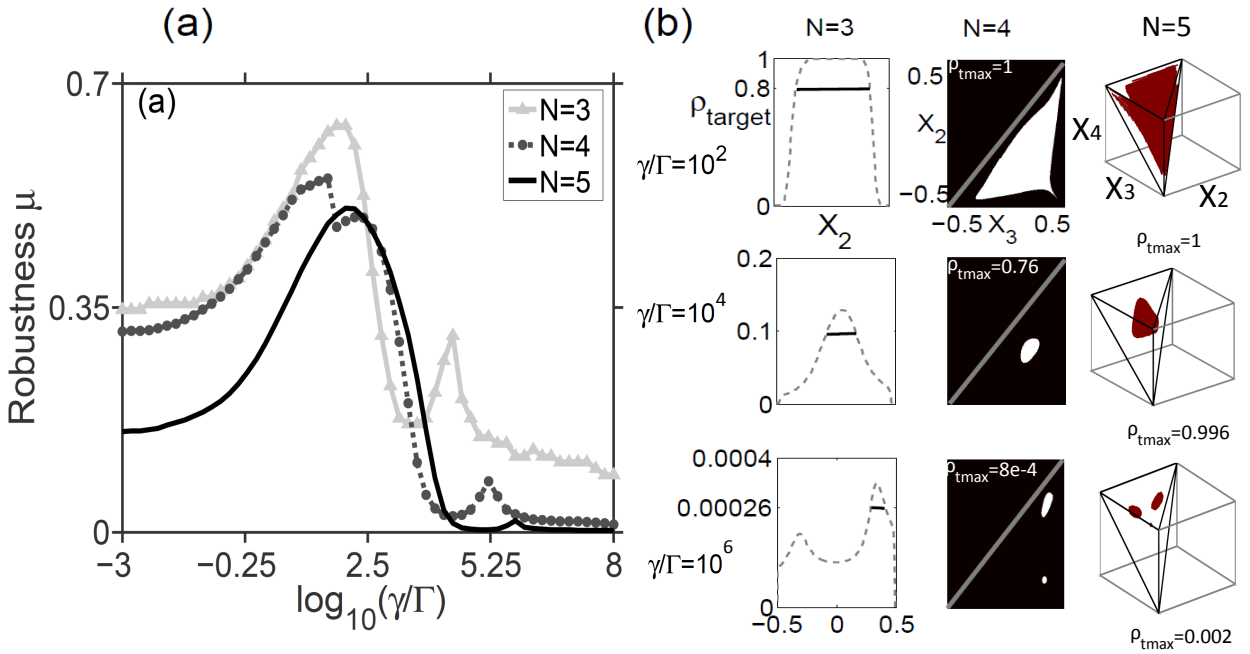

FIGURE 3.5: (Color online) Graph (a) shows the dependence of the robustness μ on dephasing noise for three different number of network sites ($N = 3,4,5$) for interaction type 1 with network parameters $VL^{-3}/\Gamma = 1$, and $T.\Gamma = 100$. It can be seen that one site to the system does not have a significant effect on the average amount of robustness however the peaks move forward down. Graph (b) shows the efficient network configurations for different dephasing noise for $N = 3,4$ and 5 which could show the behaviour of optimal configurations of arbitrary N-site networks in different regimes of dephasing noise.

effect. Fig. 3.6(b-d) shows the quantified entanglement using the same bipartite split but now in the presence of dephasing noise. It is checked that the symmetric and diagonal black configurations with no entanglement in these figures are the efficient configurations for quantum transport. For example the grey dashed triangules in Fig. 3.6 (d) show the area of efficient configurations as in Fig. 3.2(b-I). By increasing $\gamma/\Gamma \sim 10^{-2} - 10^{3}$, the maximum Log-negativity decreases and the oscillations with respect to different configurations disappear. Another characteristic shown in Fig. 3.6 is that the symmetry of non-zero entanglement area gradually breaks toward the target or the fifth site. It is clear that the lack of symmetry also exists in zero dephasing noise for some configurations with middle sites closely located to the target. However by increasing γ/Γ, the amount of Log-negativity for these configurations increases from zero to the maximum amount. This behaviour confirms that the dephasing noise has a crucial roll in determining the Log-negativity of

different network configurations.

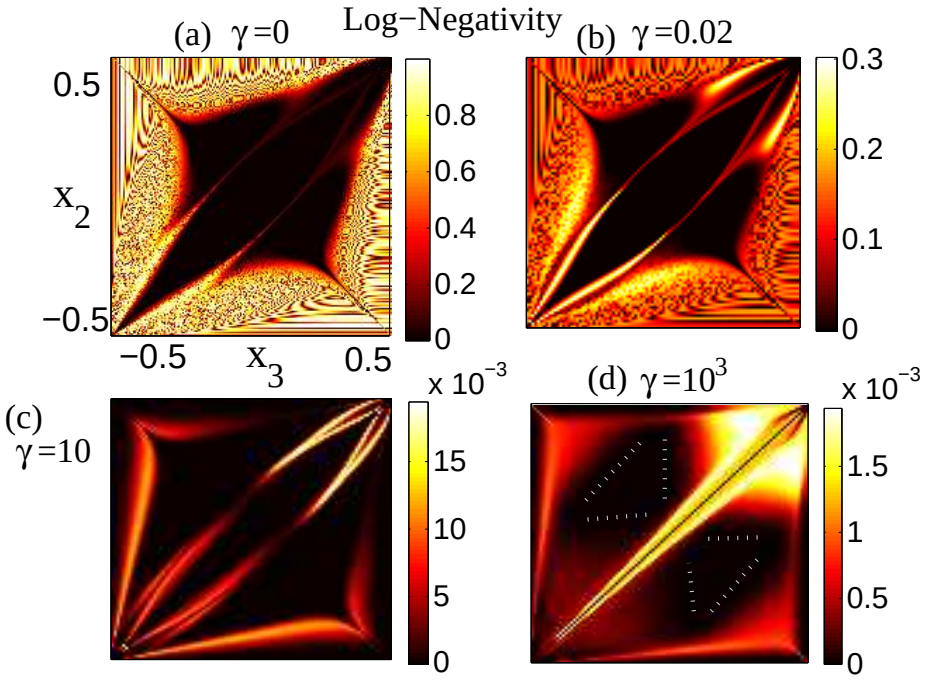

FIGURE 3.6: (Color online) Evidence of quantum entanglement in the dephased networks ($\gamma/\Gamma = 2\times10^{-2}, 10, 10^3$). Logarithmic negativity between site 1 and the rest of the network for different site couplings or network configurations are shown when the network environment parameters are considered as $\Gamma t = 100, VL^{-3}/\Gamma = 1$. The rapid oscillations of entanglement dominate mostly for poor transport network configurations in small γ/Γ, indicating the existence of trapping network geometries where the excitation is trapped in correlations within the chain. With higher dephasing noise, the Log-negativity does not oscillate and is predominant for configurations which are nearer to the last site. The black regions in symmetric areas and diagonal regions are the efficient configurations of such networks passing the excitation successfully. For large depahsing this area is shown by the grey triangular dashed lines in part(d). The change of patterns shows the strong correlation between the dephasing noise and the amount of entanglement for different classes of network couplings.

Quantumness of the system

In this section we investigate whether the increase of robustness due to dephsing noise is purely quantum mechanical or can also arrive in a semiclassical coherence-less description of the system. To check the coherence-less behaviour of the system we apply the Pauli master equation as described in [26] for a four site network of nearest neighbor interacting dipoles where the last site is connected to a target site through an irreversible transfer (rate $\Gamma = 1$). The interaction energies between the sites are considered to be $E_{ij} = 5\times10^{-3}/r_{ij}^3$, where r_{ij} is the distance between the

sites i and j, and the site energies are considered as $E_i = -\sum_{j=i\pm1} E_{ij}$ keeping the total energy of the system equal to zero. We then find the ranked eigenenergies of the total Hamiltonian of the system and the associated energy gaps between the adjacent energy levels k and l as $\Delta E_{k,l}$. In addition, a symmetric Lorentzian hopping rate between the system energy levels is considered as $1/(4\pi)1/(\Delta E_{k,l}^2 + 1/16)$, and due to the dephasing noise a Lorentzian profile for the line broadening of energy levels has been considered as ELW. To compute the average target population for a given network configuration and network parameters at $t = 100$, using the coherence-less Pauli master equation over accumulated time increments of $dt = 0.05$, we independently sampled from the Lorentzian distribution of energy levels at each time step, and averaged over 20 independent trials to arrive at a final average target population. The amounts of target population of all configurations for each different energy level width (ELW) and the corresponding geo-robustness have been found and shown in Fig. 3.7 (a). It can be seen that in lower amounts of line broadening the robustness of the system increases by increasing ELW, due to the overlap of energy levels [26] providing more paths of energy transfer. There is also a possibility of a peak of geo-robustness within the higher amounts of ELW. Fig. 3.7 (b) shows the pattern of optimal configurations of four site networks in four different amounts of line broadening of the energy levels (ELW). By increasing the line broadening further, it can be seen from Fig. 3.7 (b) that the pattern of optimal configurations gradually changes from a solid triangle to a blinking one, and so the average amount of geo-robustness decreases due to the fluctuations of target population with respect to the network geometries. In addition, it should be noted that the amount of geo-robustness changes in different points of the parameter space of both quantum mechanical and coherence-less systems, and the revival of μ can be achieved through the coherence-less Pauli master equations or the Markovian master equations.

3.1.5 Conclusions

The study of robustness of optimal configurations is useful for environment engineering of nano-networks in the Markovian regime. In this study we showed that the geometrical robustness of

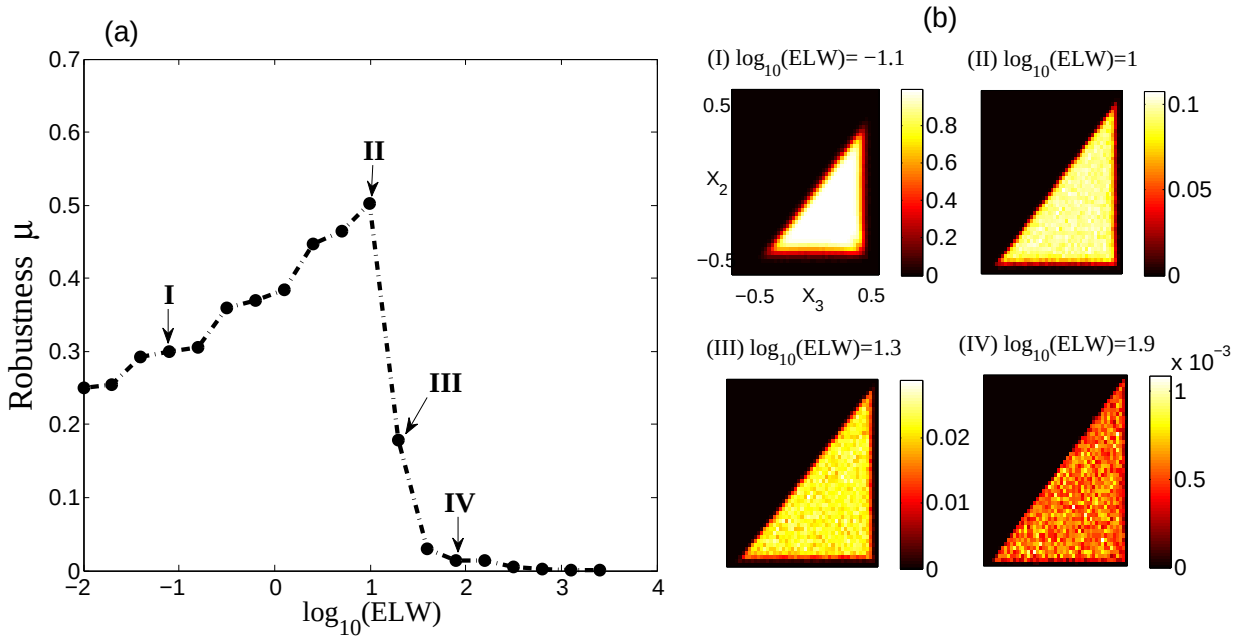

FIGURE 3.7: (Color online) This figure shows the increase of geo-robustness due to the line broadening of the energy levels analysed by Pauli master eqaution. Part (a) shows the variation of geo-robustness of a network of four nearest neighbor interacting dipoles with a Lorentzian hopping rate of $1/(4\pi)1/(\Delta E_{k,l}^2 + 1/16)$, initial interaction energies corresponding to $5 \times 10^{-3}/r_{ij}^3$, at $t = 100$, and $\Gamma = 1$, while suffering from different broadened energy levels of width ELW due to environmental collisions. However the average amounts of μ in very large energy level widths (ELW$>$ 10) are showing a peak, due to some numerical errors the decrease of ge-robustness in this range is not deterministic. Part (b) shows the optimal patterns of configurations of the same network in the presence of four different values of line broadening. It can be seen that for the chosen network parameters the increase of geo-robustness in the presence of dephasing noise qualitatively matches that observed in the quantum case.

excitation transfer (μ) in 1D networks depends on the network parameters and the environmental dephasing noise. The robustness displays two peaks with increased dephasing in specific network parameters. Increasing the number of sites of such networks typically does not change the behaviour of geometrical robustness. In addition, for both interaction types I and II, there are substantial differences in the robustness in weak dephasing noise regime. In high values of dephasing noise, the pattern of optimal configurations of such networks changes significantly from central symmetric pattern to marginal ones and the behaviour seems to be preserved for any arbitrary number of sites. In all trapping configurations of such networks the initial excitation is

accumulated in the entangled states in terms of coherences which ensures the quantum mechanical characteristics of these networks. Moreover, we have found that the increase of geo-robustness in the presence of line broadening can be qualitatively explained either through a coherence-less system or a quantum system.

3.1.6 Discussions and comments

I prepared a report analysing how network parameters affect the efficient configurations of four-site one-dimensional networks. Following the discussions with Professor Jason Twamley we noticed a peak pattern of efficient configurations within the results and proposed the idea of geo-robustness of such networks. We also compared the transport efficiencies of nearest and non-nearest neighbor interacting networks and calculated the geo-robustness for different network-environment parameters, types of site-couplings, and number of sites. The referee of the Phy. Rev. A journal suggested to compare the quantum problem with the classical one and we added the entanglement analysis to show the quantum effects of the network dynamics. I thank Professor Martin Plenio for supports regarding the initialization of this paper. This work was partially funded by the Alexander von Humboldt Foundation, and the ARC Centre of Excellence in Engineered Quantum Systems, ARC Project Number CE110001013.

4

Switching application of qubit networks

4.1 Platonic quantum networks as coherence-assisted switches in perfect and imperfect situations

4.2 Abstract

The concept of coherence switches with nanoparticle platonic networks is introduced and analysed. The platonic networks store an initially injected excitation for extremely long durations via the formation of dark states. Switching is achieved by the nano-mechanical arrangements of one site or some part of the network to remove the trapping thus leading to a highly efficient transfer

to the target which is irreversibly connected to one site. We present coherence switches based on controlling a cubic network both in the absence and presence of environment and manufacturing/topological noise.

4.3 Introduction

Photonic switches are important for integrated quantum optical networks [76, 77]. There are different mechanisms and controlling methods that switches are based on. The switching control could be all-optical [78], nano-mechanical, or a combination. In metallic nano-particle switches [79, 80] the controlling mechanism could be a combination of laser illumination and nanometric displacement. In a double core optical fibre switch, the switching mechanism is based on nano-mechanical movement of the core structure [81]. In an optical Kerr switch a nano-mechanical resonator is coupled to a quantum dot and the switching is achieved by controlling the pumping field [82]. By trapping an atom in the nearfield of a photonic crystal cavity one can create a quantum phase switch in which a photon is strongly coupled to the atom and by changing the phase of the atom or photon the other's phase can be controlled [41]. In a hybrid system by coupling the surface plasmons of a metallic nano-particle and the exitons of a quantum dot one can control the enhancement of a second harmonic signal by changing the intensity or the frequency of the pumping field [80].

In this paper we introduce a coherence-assisted photonic switch which is based on the presence or absence of dark states. The switch consists of a network of identical sites with dipolar interactions, located on the vertices of platonic geometries shown in Fig. 4.1(b). Each network can be built through state-of-the-art nano-fabrication methods like wafer thinning, metallization, and nano-lithography by positioning the sites on crossing wafers. The initially injected excitation on one site traverses through all sites while the last site is continuously discharging into the target site through a dissipative process. The switch is controlled by the nano-mechanical movement of one site or some part of the network where such nano-mechanical movement is possible through a variety of methods [83, 84]. The transfer properties of such networks for arbitrary one-dimensional geometries and ranges of interactions have been studied [85]. In this work we analytically prove

the existence of dark states for three-dimensional networks of platonic geometries connected to a target site, and show their trapping behaviours through simulations for switching usage. The presence of dark states in such networks is due to the destructive interference of the propagating excitation along different paths through to the target. The transfer properties of two possible versions of the simple cubic platonic geometry will be investigated where the associated network contains eight sites on the vertices and a target site. Moreover, a combination of two platonic networks i.e. two concentric cubes with sixteen sites will also be studied. It will be shown that by changing the position of one site or one part of the network as the controller, the initial excitation can be completely/partly trapped by the network thus blocking the transport to the target. In some configurations there is no dark state and the excitation is completely transferred to the target site. We also show that environmental dephasing and dissipation noise decreases the switching efficiency of cubic networks. However, in some specific cases, and in the presence of topological errors or large dephasing noise, some blocking/transferring network geometries are found to be useful for efficient nano-switching.

The considered platonic networks with dipolar interactions are specific and more practical examples of some general networks with suitable connectivity matrices investigated by continuous time random walk processing [86], and as such could have a broad range of applications from communication to computation [87].

4.4 Dark states in platonic networks

The system consists of N sites with one excitation initially located on site 1 at $t = 0$. The N^{th} site of the network is irreversibly connected to a target site at rate Γ. The Hamiltonian of the system excluding the target is considered as

$$H = \sum_{i=1}^{N} \varepsilon |i\rangle\langle i| + \sum_{i \neq j} J_{ij} |i\rangle\langle j|, \tag{4.1}$$

in which ε is the energy of each site, $J_{ij} = 1/r_{ij}^3$ is the dipolar coupling rate between sites i and j separated by the distance r_{ij}, and $|i\rangle$ is a state of the system indicating that the excitation is on site i. In the special case which we denote as homogeneous coupling, the coupling rate J_{ij} which is dependent on the location of site l is homogenous when other sites are all equidistant to l e.g. $(J_{il} = J_l)$, then we have

$$H|l\rangle = \varepsilon|l\rangle + J_l \sum_{i \neq l} |i\rangle. \tag{4.2}$$

Now consider another site m which has the same symmetrical feature of l i.e. $J_l = J_m$. In this case one can easily show that the antisymmetric superposition state $|l\rangle - |m\rangle$ is an eigenstate of the Hamiltonian with eigenvalue $\varepsilon - J_l$ under the conditions of homogeneous coupling. One approximation of such trapping networks is when two, or in general n_0 sites, are located close to each other so that $|r_{ij}| \gg |r_{ik}|$; $i, j \in \{1, ..., n_0\}$. Such network arrangements will be used for controlling platonic switches. Another type of dark states exists in networks of N sites where the sites l and m are symmetrically located with respect to all other sites and the coupling rate between them is J_{lm}. The Hamiltonian of Eq. (1) operates on the the state $|l\rangle(|m\rangle)$ as follows:

$$H|l\rangle = \varepsilon|l\rangle + J_{lm}|m\rangle + \sum_{i \neq l,m}^{N} J_{il}|i\rangle. \tag{4.3}$$

By subtracting $H|m\rangle$ from $H|l\rangle$ the antisymmetric trapping state of $|l\rangle - |m\rangle$ is achieved with the corresponding eigenvalue $\varepsilon - J_{lm}$. Such trapping states exist in networks with platonic geometries. To achieve switching we connect the last site to a target by an irreversible transfer process of rate Γ so that any excitation on last site will be irreversibly "dumped" to the target. This consideration will add a damping term to the N^{th} site of the system Hamiltonian [86] and the derived trapped states remain. The time evolution following the initial excitation on the first site for such networks can be found by the following Master equation with the Lindblad operators corresponding the environmental noise in the Markovian regime

$$\dot{\hat{\rho}} = -i[\hat{H},\hat{\rho}] + \mathscr{L}_{target}(\hat{\rho}) + \mathscr{L}_{dissipation}(\hat{\rho}) + \mathscr{L}_{dephasing}(\hat{\rho});$$
$$\mathscr{L}_{target}(\hat{\rho}) = \Gamma(2\hat{\sigma}_{N+1}^{\dagger}\hat{\sigma_N}\hat{\rho}\hat{\sigma_N}^{\dagger}\hat{\sigma}_{N+1} - \left\{\hat{\sigma_N}^{\dagger}\hat{\sigma}_{N+1}\hat{\sigma}_{N+1}^{\dagger}\hat{\sigma_N},\hat{\rho}\right\}),$$
$$\mathscr{L}_{dissipation}(\hat{\rho}) = \Gamma_{diss}\sum_{i=1}^{N}(2\hat{\sigma}_i\hat{\rho}\hat{\sigma}_i^{\dagger} - \left\{\hat{\sigma}_i^{\dagger}\hat{\sigma}_i,\hat{\rho}\right\}),$$
$$\mathscr{L}_{dephasing}(\hat{\rho}) = \gamma\sum_{i=1}^{N}(2\hat{\sigma}_i^{\dagger}\hat{\sigma}_i\hat{\rho}\hat{\sigma}_i^{\dagger}\hat{\sigma}_i - \left\{\hat{\sigma}_i^{\dagger}\hat{\sigma}_i,\hat{\rho}\right\}), \tag{4.4}$$

where Γ is the discharge rate of the last site N to the target site $N+1$, and Γ_{diss} and γ are the dissipation and dephasing noise rates from each site to local environments, respectively. $\hat{\sigma}_i^{\dagger}(\hat{\sigma}_i)$ is the Pauli creation (annihilation) operator for site i such that $\hat{\sigma}_i^{\dagger} = |i\rangle\langle 0|$. The state $|i\rangle$ denotes one excitation on site i, and the state $|0\rangle$ represents the zero energy excitation of the network while the initial energy has been dissipated to the environment.

By measuring the population of the target by Eq. (4.4) we can gauge the efficiency of the transferring/blocking through the network. Fig. 4.1(a) shows all five possible platonic networks with unit edge lengths in which the nearest neighbour sites are equidistantly located on a sphere. The numerical graphs of Fig. 4.1(b) show the target population in time for each platonic network with no environmental dissipation or dephasing noise. The self-energies of sites are considered zero for the whole chapter ($\varepsilon = 0$). The trapped excitation within the networks can be found by subtracting the target population from the initially injected energy. The spheres on the vertices of the networks of Fig. 4.1(a) show the average amount of excitation trapped on each site after a long time interval. It can be seen that in all cases, except the four site tetrahedron network, most of the excitation is trapped within the first site and a *symmetric* site which is symmetrically located to that site with respect to the center of the platonic network. According to Eq. (3) each pair of *symmetric* sites (i,$\tilde{i}$) that are in a same relative distance from all other sites, create a trapping state of $|i\rangle - |\tilde{i}\rangle$. As the entire excitation is initially on site 1, the average trapped excitation will mostly remain in the antisymmetric state of $|1\rangle - |\tilde{1}\rangle$. Since the N^{th} site is discharging continuously into the target, the

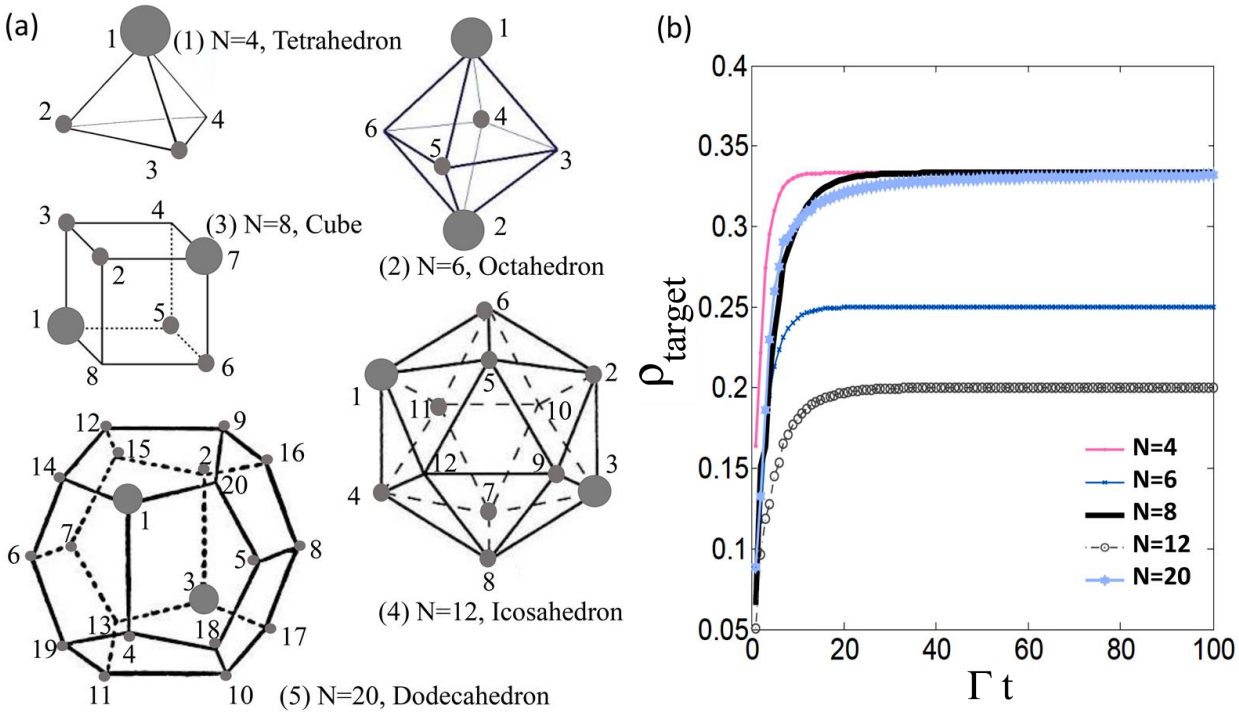

FIGURE 4.1: Graph (a) shows the five platonic quantum networks with unit edge length. These networks consist of identical sites located at the vertices of the five regular platonic solids where we label the sites as shown. Site 1 in each network is initialized with one energy excitation and the N^{th} site is connected irreversibly to a target at rate Γ. The gray spheres depicted on some sites show the average population of excitation on the sites after a long evolution time of $\Gamma t = 1500$ that indicate the existence of preferential trapping sites. Graph (b) shows the target population of each network versus time in the absence of environmental noise.

averaged trapped excitation on sites $N, \tilde{N}$ are zero. It has been checked that by changing the position of the last site this rule persists and the average populations of other sites do not change. In other words, due to the wave nature of the excitations, such super-symmetric 3D networks behave as a spherical mirror bouncing the launched excitation between the first and its symmetric site for a long time.

Now we try to find an analytical expression for the amount of accumulated excitation on the target. In non-nearest neighbour interacting networks that are all equally coupled to each other and irreversibly connected to a target i.e. fully connected networks (FCNs), the target population can be calculated by the expression $\rho_{target}(\infty) = 1/(N-1)$ [26]. On the other hand, the couplings in our non-nearest neighbour interacting platonic networks are distant dependent which indicates that

they are not FCNs. Here we show that due to the symmetric configurations of platonic networks, the target population obeys a rather similar expression to that of FCNs. Fig. 4.2 shows the time

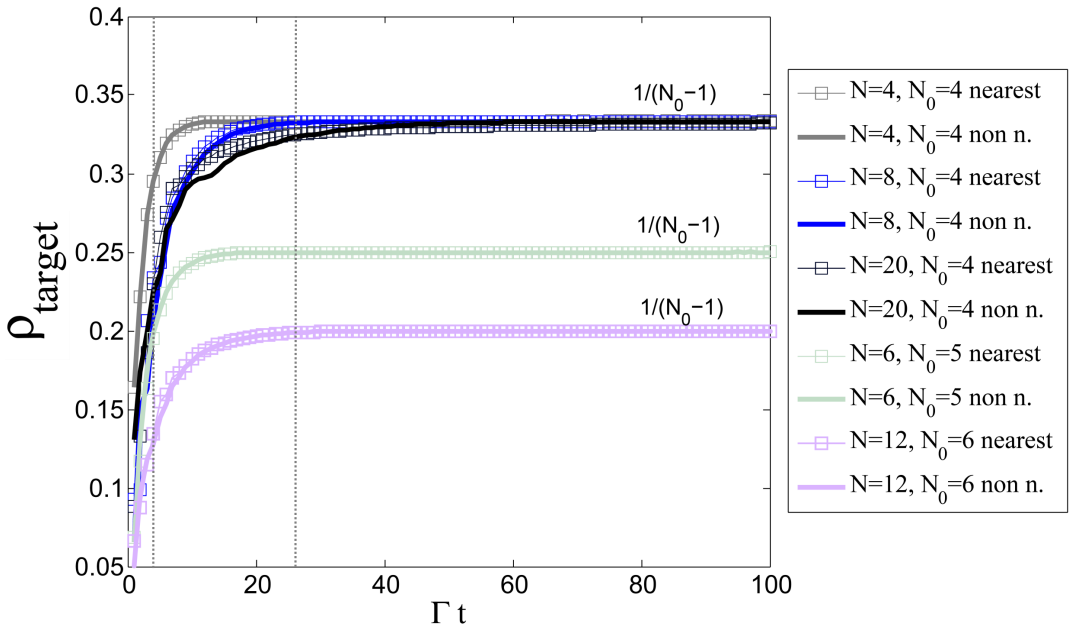

FIGURE 4.2: The target population of platonic networks for nearest neighbour and non-nearest neighbour (non n.) interactions. N is the number of sites in platonic networks and N_0 is the "equidistant coordination number" i.e. the number of nearest neighbour sites connected to each site plus the site itself. We observe that the steady state target population of each network is primarily a function of the corresponding equidistant coordination number.

variation of the target population of each platonic network for two interaction ranges indicated by nearest neighbours and non-nearest neighbours. It can be seen that the target population is not sensitive to the type of interaction and the corresponding graphs coincide almost in all cases. However there is an exception for $N = 20$ for which the graphs of two types of interactions partly deviate from each other when $\Gamma t \in (5, 27)$. The equality of target population for nearest and non-nearest neighbour systems is due to the symmetric configurations of such networks and remains unchanged at longer time intervals or different irreversible rates to the target. The same effect has been observed for target population dynamics of one-dimensional symmetric four-site networks, however for non-symmetric configurations the target population dynamics of nearest and non-nearest neighbour interactions are significantly different for specific network parameters [85].

Now by neglecting the non-nearest neighbour interactions in platonic networks, it is shown in Appendix 1 that the steady state target populations obey the relation $\rho_{target}(\infty) = 1/(N_0 - 1)$, where N_0 is a type of "equidistant coordination number" for the platonic networks i.e. the number of nearest neighbour sites equidistantly connected to the site and also counting the site itself. For example according to Fig. 4.1(a), each site on tetrahedron, cube, and dodecahedron networks has three nearest neighbours yielding a unique equidistant coordination number of $N_0 = 4$ and the same target population of $1/3$ for all of these three platonic networks.

In summary, as all nearest neighbour interacting sites in platonic networks are equally connected to each other and the non-nearest neighbour interactions are cancelled due to the symmetry, the target population of platonic N-site networks is the same as that of FCNs with only N_0 number of sites.

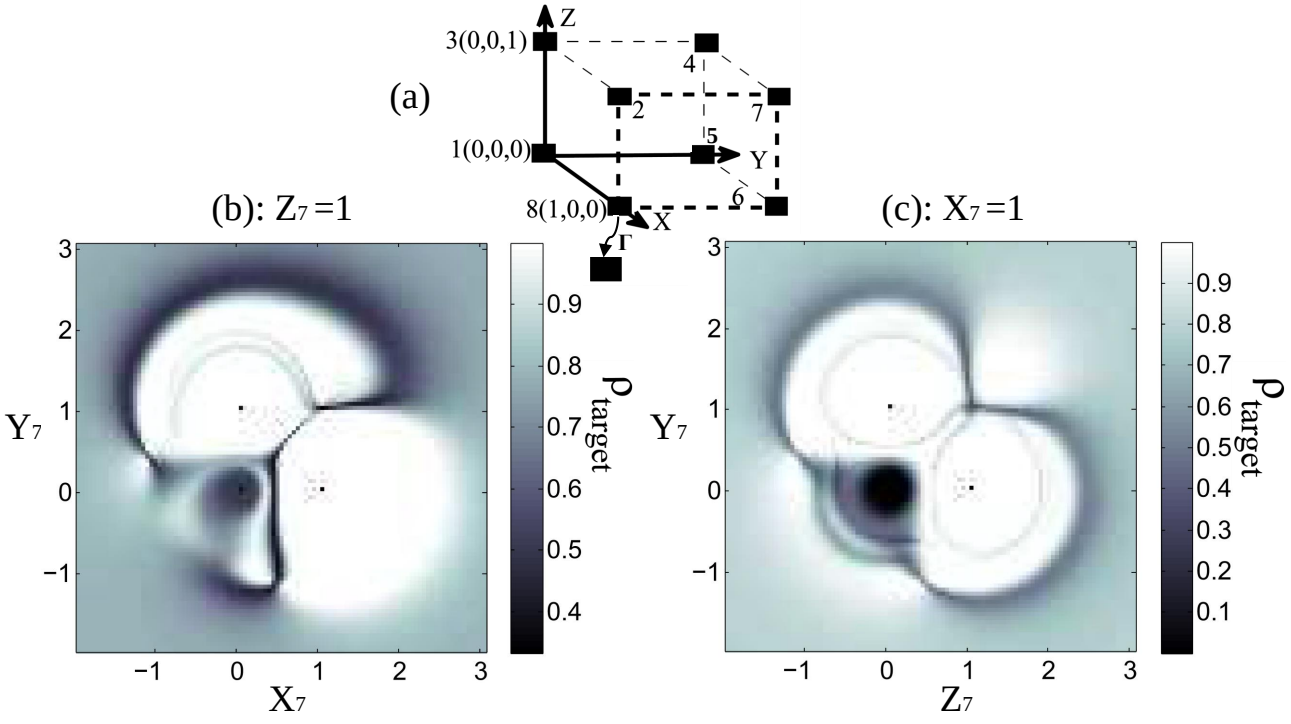

FIGURE 4.3: Graph (a) shows the schematic of cubic networks where the last site is irreversibly connected to a target sites. The target population of this network is calculated when the 7^{th} site moves in the plane $Z_7 = 1$ (graph (b)) and in the plane $X_7 = 1$ (graph (c)). It is shown, and has been independently checked for sites 1 and 5, that by putting the controller site 7 close to sites 2,4,5, and 6, the target population approaches 1 (switch ON state), while by locating site 7 around sites 1, 3, and 8 the target population decreases significantly (switch OFF state).

4.5 Cubic switches

Here we analyse a platonic cubic network which is an easy 3D geometry to build. The schematic is shown in Fig. 4.3(a) where the last site is connected to a target site at rate Γ. The target population of this network is shown on Figs . 4.1 and . 4.2. Fig. 4.3(b) and (c) show the target population when the 7^{th} site of the cube moves within the planes $Z = 1$ and $X = 1$, respectively. Fig. 4.3(b) indicates that by approaching site 7 as the switch controller to sites 2 and 4, the target population increases to unity, however by positioning the controller site to the vicinity of the third site, the target population decreases to the minimum amount. In addition, the bright areas around sites 2 and 6 in Fig. 4.3(c) show other possible positions of the controller yielding perfect transport i.e. switch ON state, that are quite robust against the position variation of the controller site. All dark regions of Fig. 4.3(b,c) are examples of switch OFF configurations or trapping regions that can be achieved by changing the position of the controller site.

The inset of Fig. 4.4(a) shows another possible cubic network in which a solid gray part of 6 sites could be displaced by dy along the positive Y axis through nano-mechanical procedures. Fig. 4.4(a) shows the target population versus time in units of Γ^{-1}, for different positions of the gray network (gn) controller which is $Y_{gn} = 1 + dy$. It shows that by increasing $|dy|$ the accumulated excitation at target gradually increases indicating that the trapping conditions are not satisfied at $Y_{gn} \neq 1 (dy \neq 0)$. Fig. 4.4(b) shows the target populations at two long time instances $\Gamma t = 100, 200$ (solid and dashed lines) for a continuous range of dy. It indicates that there is another trapping state around $dy = -1$ where sites 5 and 6 are closely located to sites 1 and 8, respectively. This trapping configuration is an approximation to the formerly introduced trapping state of closely located sites of Eq. (2). In addition, Fig. 4.4(b) shows some other tiny trappings around $dy = -2 (Y_{gn} = -1)$ corresponding to a new symmetric network. Now we study the effect of environmental noise as well as manufacturing disorders on the efficiency of cubic networks. Dephasing and dissipation environmental noise can be applied to the system through the open quantum system approach of

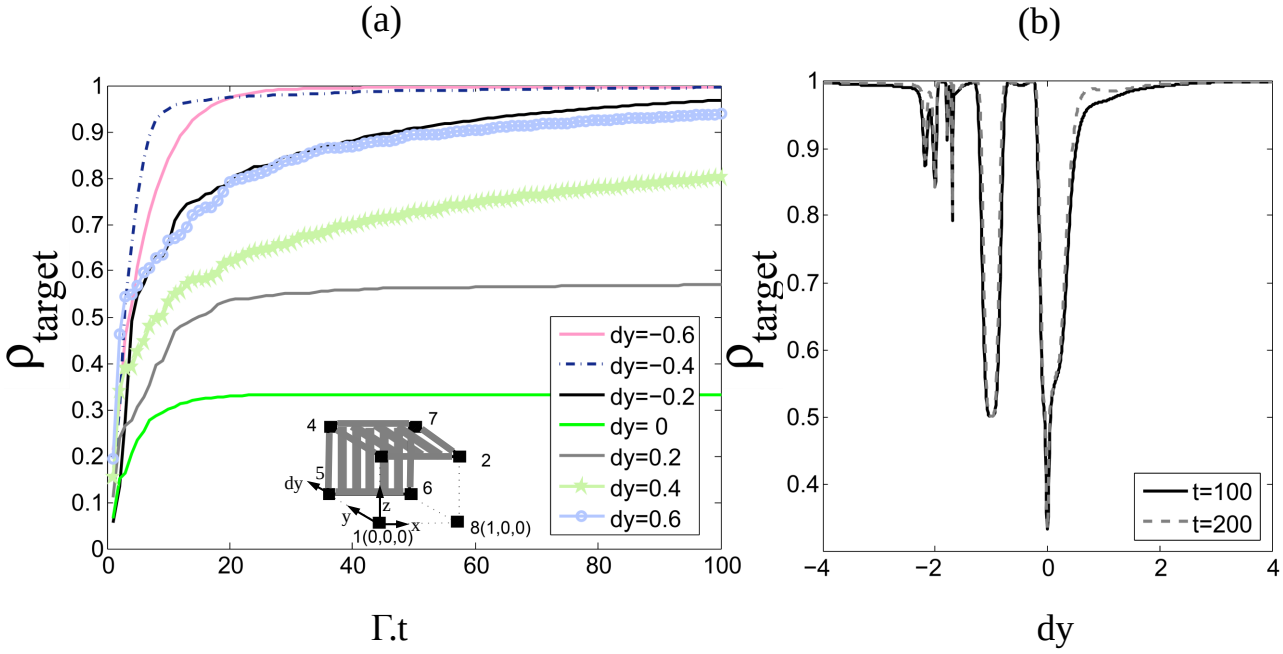

FIGURE 4.4: Graph (a) shows the target population versus time for the depicted network of the inset. dy is the position of the gray solid part of the network consisting of 6 sites moving along the Y axis. At $dy = 0$ the network configuration is a cube with a permanent dark state. Graph (b) shows the variation of target population with different positions of the solid part controller at two different instances of time $\Gamma t = 100, 200$. It shows that around three values of dy the initial population is partly trapped within the network and can yield a switch OFF configuration.

Eq. (4). These noises could be the result of elastic or inelastic collisions of network sites with surrounding particles, respectively. It has been numerically checked that the trapping states of perfect cubic switches are highly disrupted by dephasing noise so that adding a tiny amount of dephasing could significantly increase the transport efficiency. On the other hand, it has been checked that the environmental dissipation noise, which leaks the energy excitation of the system to the surroundings, has a much less disturbing effect on the dark states of cubic networks. Fig. 4.5(a) and (b) show the target populations of the cubic networks versus relative dissipation noise rates of Γ_{diss}/Γ, for different positions of site 7 and the gray network, respectively. By increasing the dissipation noise rate, at each specific Γ_{diss}/Γ the contrast between the bright and dark regions (switch ON and OFF configurations) decreases leading to smaller ON/OFF switching ratios.

A further type of noise could be due to manufacturing imperfections. For example, one site of a

platonic network could be missed or due to some environmental disorders an inter-site interaction could be blocked randomly. The Euler number represents the topological character of the platonic geometries and this Euler characteristic will change with such manufacturing errors leading to topological noise. Fig. 4.5(c) shows the transport efficiency of a cubic network with two mentioned types of topological errors occurring with probabilities p_0. It can be seen that by applying such topological noises to a perfect cube network, the target population increases with increasing topological error rate p_0. It is curious to note that the increase is more dramatic in the case where one link alone is removed rather than one vertex. It is likely that the second type of manufacturing error greatly restricts the transport flow through to the target site. The black graph of Fig. 4.5(c) shows the effect of topological noise of the first type on target population of a deviated cubic network with the 7^{th} site located close to the 8th site. It shows that the excitation transport to the target is not very sensitive to the probability of the topological noise. We thus observe a wide variety of behaviours of the transport depending on the types of environmental and topological noise.

4.6 Concentric cubic switches

In this section we show that the combination of two platonic networks (two concentric cubes) enhances the switching ON/OFF ratio in comparison with one platonic network and this ratio is robust against environmental dephasing noise so that for large dephasing rates the large switching ON/OFF ratios are retained. We suppose a network of 16 sites located on the vertices of two concentric cubes while one of the cubes is rotated around axes x, y, and z by angles $(\theta_X, \theta_Y, \theta_Z)$. The first site of the network that initially contains one excitation is a nearest neighbour of the last site on the same cube which is irreversibly connected to a target site at rate $\Gamma = 1$.

Fig. 4.6(a) shows the population accumulated at target until $\Gamma t = 100$, for different network configurations indexed by $(\theta_Z, \theta_Y, \theta_X = \pi/4)$. The switching ON and OFF states are network configurations for which the target populations are most significantly different from each other and could be obtained by changing the orientation of one cube or the position of one site as switch controllers. It can be confirmed from Fig. 4.6(a) that the best achievable switching ON/OFF ratio of this network

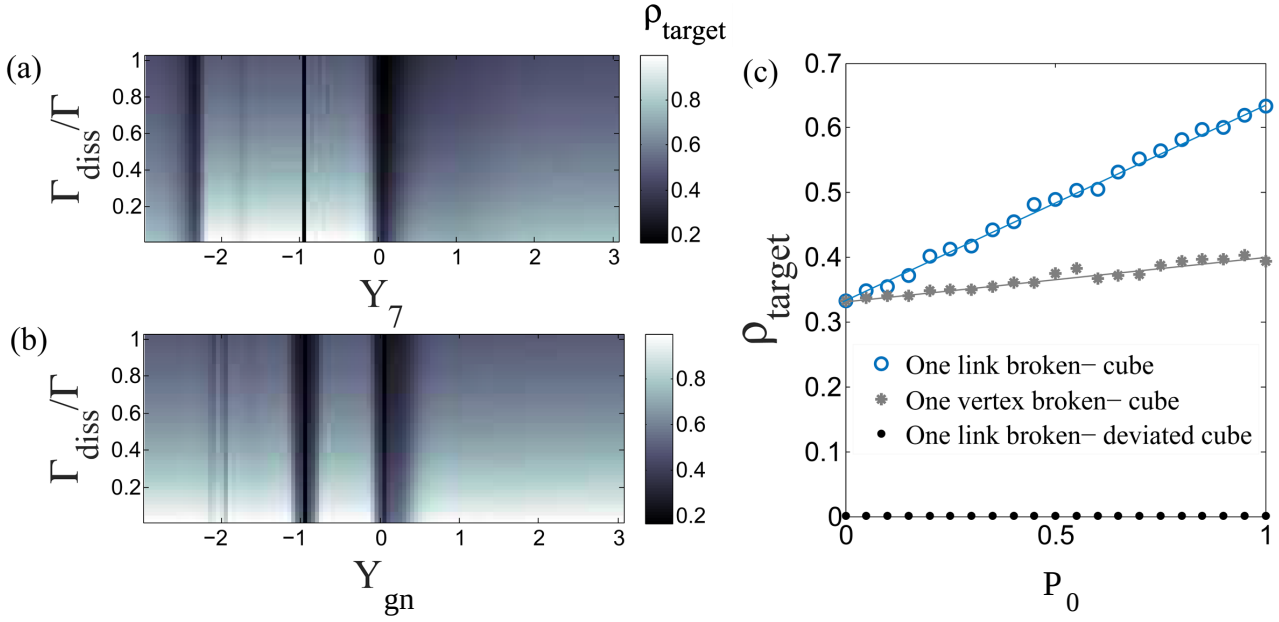

FIGURE 4.5: The target population of cubic networks in the presence of dissipation and topological noise: Graphs (a) and (b): the transport efficiency of cubic networks with different positions of site 7 and the gray network along the Y axis, respectively. It is observed that by increasing the dissipation noise the switching ON/OFF ratio decreases in both cases. Graph (c): the target population of cubic networks in the presence of topological errors characterised by a factor p_0. The blue marks correspond the cubic networks with one randomly broken link, the gray marks correspond cubic networks with one randomly removed site with three missing nearest inter-site interactions, and the black marks correspond a deviated cubic network with site 7 positions near site 8. Each point has shows the average value of the target population of 1000 networks with each of these topological error types occurring with probability p_0. It can be seen that by increasing the topological noise probability, the average trap states of both types are disturbed in cubic networks leading to an increase of the transport efficiency. However the trapping excitation of the deviated cube networks is not disturbed by increasing topological or dissipation noises.

would be 1 while the switch ON state is a network configuration with target population of 1 and the OFF state has the target population of zero. Fig. 4.6(b) shows the target population of a two concentric cube network when the second cube has been rotated by $(0,0,\theta_Z = \pi/4)$ and the 3^{rd} site as the controller is moving in the plane $Z = 0.5$ with the origin of coordinates at the center of the cubes. It can be seen that by changing the position of the 3^{rd} site $(X_3, Y_3, Z_3 = 0.5)$, the population of the target increases from zero to one. Fig. 4.6(c,d) show the target population of the concentric cubes network of parts (a) and (b) in the presence of a large relative dephasing noise

rate $\gamma/\Gamma = 100$. This result indicates that the considered superposition of platonic networks exhibit high switching contrasts even in the presence of large dephasing rates.

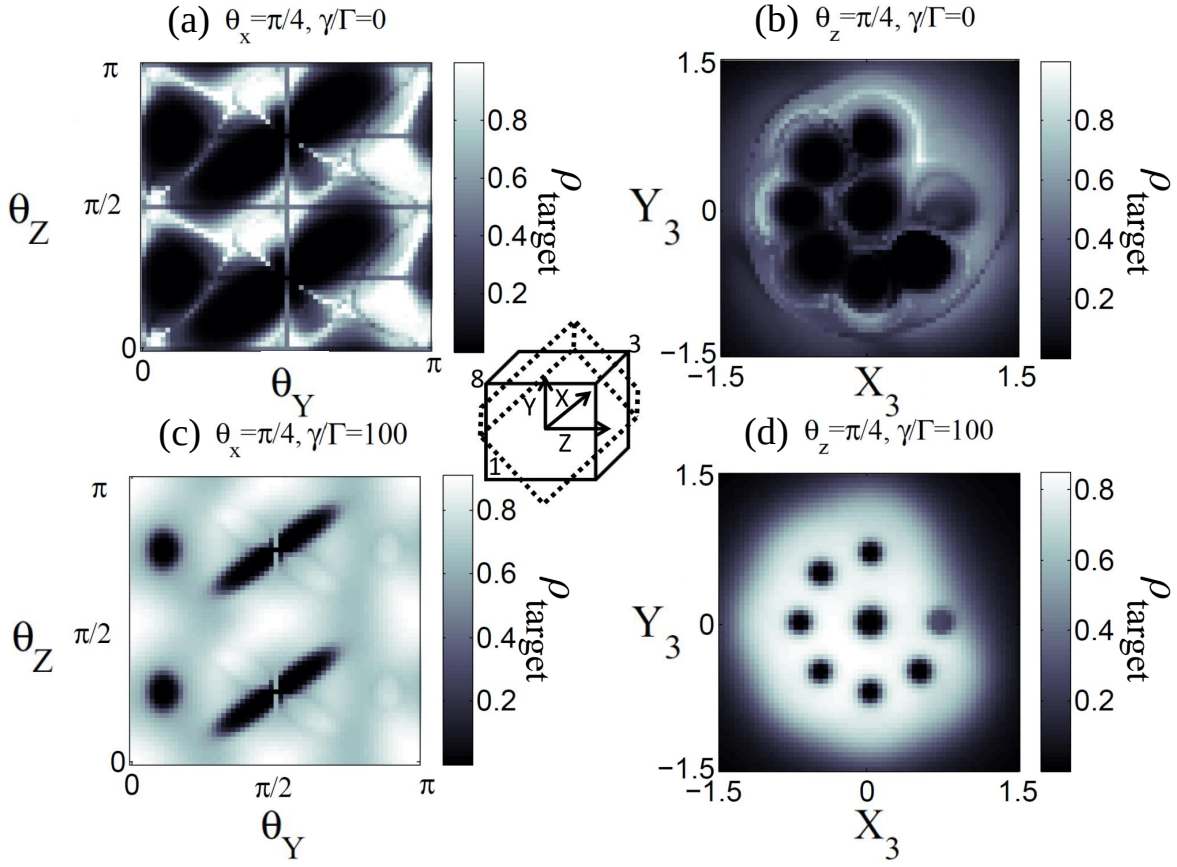

FIGURE 4.6: Target populations of a network of 16 sites located on the vertices of two concentric cubes evaluated when $\Gamma t = 100$ where the 8^{th} site is connected to the target. In graphs (a) and (c) the second cube as the switch controller is rotated by angles $(\theta_X, \theta_Y, \theta_Z)$, and in graphs (b) and (d) the position of the 3^{rd} site moves in the plane $Z_3 = 0.5$. Graphs (c) and (d) show the transport efficiency of the networks in (a) and (b), respectively, in the presence of dephasing noise of rate $\gamma = 100\Gamma$. This shows that even with significant dephasing noise such combined platonic networks possess high switching contrast.

4.7 Conclusion

We have shown that a platonic network can partly store energy excitations for a long time using dark states within the network. The degree of trapping we observed follows the corresponding relation in arbitrary fully connected network with all sites equally connected to each other. We suggested that coherence-assisted trapping of such platonic networks could have switching applications for miniaturized structures. It is shown that by changing the position of one site, or a part

of the network, in the absence and presence of environmental noise, the target population varies from a minimum amount to unity which can be considered as switch ON/OFF states. Here we have considered the first and the target sites as the input and output ports of the switch. In future it may be also possible to have a switchable irreversible energy rate not only connected to the last site but also connected to all sites, and as generally discussed in [86], to obtain a multi output port platonic switch.

4.8 Appendix 1

In this appendix the solution of the Master equation for the target site population of a platonic network will be given. Eq. (4) can be written in exact terms of density matrix elements as following

$$\dot{\rho}_{ij} = -[2\Gamma_{diss} + \Gamma(\delta_{iN} + \delta_{jN}) + 2\gamma - 2\gamma\delta_{ij}]\rho_{ij} - i(\sum_{l\neq i,j}^{N} J_{il}\rho_{lj} - \sum_{l\neq i,j}^{N} \rho_{il}J_{lj}), \tag{4.5}$$

$$\dot{\rho}_{00} = 2\Gamma_{diss}\sum_{j=1}^{N}\rho_{jj}, \tag{4.6}$$

where $J_{ii} = \varepsilon$, and ρ_{00} is the population of the ancilla site accumulated due to the local dissipation noise of rate Γ_{diss} applied equally to all sites. For a platonic network with equidistant coordination number of N_0 (the number of sites equidistantly located around each site), Eq. (5) can be written as

$$\dot{\rho}_{ij} = -[2\Gamma_{diss} + \Gamma(\delta_{iN} + \delta_{jN}) + 2\gamma - 2\gamma\delta_{ij}]\rho_{ij} - iJ(\sum_{l=f(j)} \rho_{lj} - \sum_{l=f(i)} \rho_{il}), \tag{4.7}$$

where $J = v/r_{il}^3$(or v/r_{lj}^3) is the equal couplings between site i (or j) and its $N_0 - 1 (= N_e)$ equidistant neighboring sites indexed by $f(i)$(or $f(j)$). For example the node site $i = 4$ in the octahedron platonic network depicted in Fig. 4.1(a-(2)) is connected to four nearest neighbouring sites ($N_e = 5$) with coupling rate J with indices $f(i = 4) \in \{1, 2, 3, 6\}$. Now we define a set of collective variables

as following

$$R_i = \sum_{j=f(i),i,N} \rho_{ij}, \qquad \Lambda = \sum_{i=f(i),i,N} R_i. \tag{4.8}$$

where for a node site i in the vicinity of the N^{th} site, $f(i)$ takes the values of a set of $N_e - 1 (= N_0 - 2)$ indices. By re-expressing Eq. (7) in terms of the collective variables for a node including the N^{th} site, Eq. (A3) of [26] is found where $\Gamma \to \Gamma_{diss}$ and $\Gamma_{N+1} \to \Gamma$. Then by substituting N by N_0 Eq. (A4) and (A5) can be obtained which are the first equations including the number of sites. The rest of the proof can be exactly followed up to Eq. (A15) of [26]. Consequently, the target population of platonic networks with equidistant coordination number N_0, in the absence of environmental noise ($\Gamma_{diss} = \gamma = 0$) yields

$$\rho_{target}(\infty) = 1/(N_0 - 1). \tag{4.9}$$

4.9 Discussions and comments

In a report I showed that the cubic and two attached tetrahedron networks can permanently trap an initially injected excitation. I suggested to use them for switching and proposed two methods for controlling the ON/OFF cubic switch states. Professor Jason Twamley suggested to study the transport efficiencies of more general symmetric networks with platonic geometries as well as investigating the effect of coupling range in terms of nearest and non-nearest neighbor interactions. We numerically showed that all platonic networks can permanently trap some part of an excitation, and could analytically prove the formula of the amount of trapped excitation. The referee of J. Phys. D: Appl. Phys. suggested to study the effect of topological noises and we proposed a practical method to study them. This work was partially funded by the Alexander von Humboldt Foundation, and the ARC Centre of Excellence in Engineered Quantum Systems, ARC Project No. CE110001013.

5

Conclusion

The general topic of quantum transport in qubit networks is introduced in section I. In the following sections we theoretically studied controlled quantum transport in site networks. The networks of our interest consist of short/long range interacting (mostly dipolar coupled) qubits exposed to Markovian environments where one qubit is irreversibly connected to an extra one. Two different approaches towards controlled quantum transport are studied such as efficient quantum state transfer, and switching of quantum transport between two points of such networks.

5.1 Efficient quantum transport in qubit networks

We studied efficient quantum transport from two points of view. In the first section we present the results regarding the spatial dimension preference of network configurations for efficient quantum transport, while the robust configurations analysis for efficient quantum transport is discussed with two different methods in the second and third sections.

5.1.1 Spatial dimension analysis for efficient network configurations

Regarding network dimensionality we compared the transport efficiency of networks expanded in different spatial dimensions. In the absence of environmental noise we thoroughly searched the network parameters space of the strength of site couplings and the time of measurement. We found that for specific choices of such network parameters the two-dimensional dipolar four-site networks are $O(10^{-2})$ more efficient than the one-dimensional equivalent networks. In addition, for a specific choice of network parameters we showed that the two-dimensional networks with five to eight number of sites are also $O(10^{-2})$ more efficient than their one-dimensional equivalent networks. Our results empirically assure that one-dimensional channels are adequate to achieve efficient quantum transport and designing two-dimensional networks should only be considered where the two-dimensional spatial expansion is demanded.

In a new approach towards dimension analysis we proposed a new type of qubit networks for which the two-dimensional versions are much more efficient than the one-dimensional ones: Π-chain networks are an array of equidistantly positioned dipolar coupled qubits that are displaced a perpendicular distance h (chain height) from the line connecting the first and last sites. For a specific choice of network parameters we showed that the off axis chain is $O(10^{-1})$ more efficient than the on axis chain. So to transfer a quantum of energy within an equidistantly positioned qubit chain, some two-dimensional Π configurations are much more efficient than putting the straight chain along the first and last qubits.

5.1.2 Robust efficient configurations of site networks

A brute optimization of the network geometry even in the case of success may not always lead to a robust network configuration. So the robust transport analysis is an alternative for the rough optimization algorithms searching the complex large-dimensional geometrical parameter spaces.
To achieve robust efficient configurations against the geometrical variations we calculated the transport efficiencies of one and two dimensional arrangements of qubits and presented some robust efficient patterns of configurations. Regarding one-dimensional networks, it has been shown that there are two classes of efficient configurations in four-site networks indicated as the pair and symmetric arrangements of the two interior sites. By changing the network parameters of coupling strength and the time of measurement the robust optimal patterns remain identical and only the extension of the patterns in geometrical parameter space or the maximum efficiency of the pattern changes.
Regarding one-dimensional networks with larger number of sites we showed that the pair and symmetric patterns are still the robust efficient configurations but for the last four sites of the networks where the other interior sites are located in the network center.
For two-dimensional networks consisting three qubits it is shown for a specific choice of network parameters that the surrounding network area are efficient except three inefficient circular regions around the first and third sites which trap the initial excitation within the network. By changing the network parameters of coupling strength and time of measurement the inefficient surface areas expand or shrink accordingly. Regarding two-dimensional networks including five or larger number of sites, the inefficient patterns are as those of three-site networks while the extra interiors sites are located close to each other.
The efficient patterns of two-dimensional four-site networks are more diverse as shown in the attached MP4 file of the film. It can be confirmed from the film that there are at least two robust inefficient areas around the first and fourth sites as in two-dimensional three-site networks. Changing the network parameters of site couplings and the time would only change the efficiency and

extension of the inefficient areas. It has been also shown for two frames of the film that the patterns of efficient configurations remain identical by increasing the number of sites while the additional sites are located close to each other.

In general, by adding a cluster of closely located n sites to a two-dimensional network (including one-dimensional ones), the patterns of optimal configurations only change locally.

5.1.3 Geometrical robustness of site networks

Another approach for robustness analysis is by defining a quantity as the geometrical robustness (geo-robustness) of qubit networks. By optimising geo-robustness against the network-environment parameters efficient transport is achieved with most arbitrary arrangements of the network sites. The geo-robustness is defined as the percentage of network configurations passing the initial excitation through the network as %80 of that of the optimal one.

The effect of a large variety of network parameters like the strength of site couplings, types of coupling (dipolar, van der Wals, etc), time of measurement, dephasing noise rates, and the number of sites has been investigated on the geo-robustness of the system. It has been shown that for one-dimensional four-site networks there are two peaks of geo-robustness in different network-environmental parameter regimes. The position of the optimal geo-robustness depends on the network-environment parameters. For instance, by fixing all parameters and increasing the dephasing noise the geo-robustness significantly increases. This is due to the fact that the dephasing noise broadens the system energy levels and provides additional pathways for quantum energy passing the system. So in larger dephasing noise rates more configurations are close to optimal and the geo-robustness increases. Another example is that by increasing the number of network sites, the peaks of geo-robustness shift forward with respect to the dephasing noise rate while other parameters are fixed. Such results could be used in robust one-dimensional network design for different network parameters implemented by different physical networks.

On the other hand, we checked the behaviour of geo-robustness in coherence-less systems where the hopping rates between the adjacent energy levels of the system obey a Lorenzian profile and

the dephasing noise rate is considered as the width of broadened Lorenzian energy levels of the system. For a given choice of network-environment parameters of such four-site one-dimensional networks we showed that the increase of dephasing noise will increase the geo-robustness as that of the equivalent quantum network.

5.2 Switching of quantum transport in site networks

Switching the quantum pure states between two points of quantum networks is another goal towards controlled quantum transport. We studied the transport characteristics of highly symmetric three-dimensional qubit networks called platonic networks and showed that some of the initially injected quantum of energy is stored in the network for long durations via the creation of dark states. We proved that the population accumulated in the target site after an infinite time is $1/(N_0-1)$ where N_0 is the number of equally distant neighbouring sites. So the trapped population within platonic networks is $(N_0-2)/(N_0-1)$. On the other hand, it is shown that by changing the position of one site or a set of sites (as a controller) the efficiency of the transport reaches the unity. So the ON-OFF switching states can be achieved by changing the position of the controller site within such coherence-assisted switches. However the transport efficiency of platonic switches are highly disrupted with environmental dissipation or dephasing noises, it has been checked that by combining two platonic switches, for example two concentric cubes, the switching efficiency remains unity even in very high dephasing noise rates.

Another proposed type of switching network is a Π-chain with a specific number of sites. It has been shown that for some heights of the Π-chain networks the initially injected excitation is completely trapped within the network so that the target population remains zero. On the other hand, the height of Π-chain can be adjusted to achieve the maximum transport to the target site. This characteristics can be used for switching quantum transport within the first and last sites.

5.3 Future directions

In this thesis we considered networks consisting two-level systems where one site is irreversibly connected to another two-level system. A possible future route of enquiry is considering qubit networks without the irreversibly connected sites and investigate perfect and permanent transfer of quantum information. Such quantum transport can be achieved by engineering the dynamics of the interior sites. It can be shown that such dynamic networks can permanently transfer an entangled state within two closely located sites to the two other sites located in a different position and the distance of transport can increase by adding the number of interior sites.

Another possible investigation is considering a qubit network in which different sites are irreversibly connected to distinguished target sites. It can also consider that one or a few source sites are irreversibly discharging to some sites. Such networks can be investigated as multi-port switches that are vital for quantum communication and computation purposes.

A

Appendix 1

A.1 Comparison of transport efficiencies of one and two-dimensional networks

Here the optimal target population of site networks is found via the random walk optimization code presented in section 2.1.3. Different network-environment parameters are considered as dissipation noise rate (Γ) and dephasing noise rate (γ), coupling strength (V), measurement time (T), dissipation noise rate from the last site to the target site or sink (Γ_{sink}). In order to realize whether the

two-dimensional networks are more efficient than one-dimensional ones, we search through different configurations of one and two-dimensional networks via the random walk optimization procedure and compare the maximum target population of the one-dimensional and two-dimensional networks ($\rho_{sink1D-max}, \rho_{sink2D-max}$). Tables A.1-A.4 presents the cases of network parameters for which the two-dimensional four-site networks are more efficient than the one-dimensional ones. In each case, the first and last sites are located at $x_1 = -1$ and $x_N = 1$ and the other sites which are coupled via dipolar interaction are positioned within these sites as in section 2.1.3. To effectively search through the network-environment parameter space the product of some variables like Γ_{sink} and T) is kept constant. It can be confirmed from Tables A.1-A.4 that for network parameters $[\Gamma_{sink} = 0.7, V = 1, T = 7.143, \gamma = 0, \Gamma = 0]$ the maximum difference of transport efficiency of two and one-dimensional networks is $\delta\rho_{21} = 0.012111$.

$[\Gamma_{sink}, V, T, \gamma, \Gamma]$	$\delta\rho_{21}$	$\rho_{sink1D-max}$	$\rho_{sink2D-max}$	x_1, x_2	$(x_1, y_1), (x_2, y_2)$
$\Gamma_{sink}.T = 5,\ [0.5, 1, 10, 0, 0.01]$	0.001529	0.910242	0.911292	-0.1929,0.3499	$(0.2109, -0.1522)$, $(0.3399, -0.0566)$
$\Gamma_{sink}.T = 5, [0.6, 1, 8.33, 0, 0]$	0.006992	0.962838	0.969831	$-0.2029, 0.2702$	$(0.2727, 0.1631)$, $(-0.2209, 0.5113)$
$\Gamma_{sink}.T = 5, [0.64, 1, 7.812, 0, 0]$	0.011218	0.962549	0.973767	-0.186749, 0.342074	$(0.2506, 0.7562)$, $(-0.2718, 0.3135)$
$\Gamma_{sink}.T = 5, [0.7, 1, 7.143, 0, 0]$	0.012111	0.962097	0.974209	$0.2849, -0.2031$	$(0.2710, -0.2665)$, $(-0.2593, -0.6908)$
$\Gamma_{sink}.T = 5, [0.72, 1, 6.94, 0, 0]$	0.011672	0.962347	0.974019	$-0.1999, 0.3451$	$(0.2518, -0.1870)$, $(-0.2359, -0.6508)$
$\Gamma_{sink}.T = 5, [0.74, 1, 6.76, 0, 0]$	0.008687	0.963368	0.972055	$-0.1966, 0.3491$	$(-0.3232, 0.7736)$, $(0.3345, 0.4529)$
$\Gamma_{sink}.T = 5, [0.8, 1, 6.25, 0, 0]$	0.007851	0.963146	0.970997	$-0.2065, 0.34990$	$(-0.2800, -0.7202)$ $(0.2744, -0.2730)$

TABLE A.1: This table shows for the chosen network-environment parameters that the two-dimensional qubit configurations are more efficient than the one-dimensional ones. The product of two network parameters is kept constant and equal to 5. The first and fourth sites of the networks are fixed at $-1, 1$ and the optimized coordinations of the two interior sites of one and two-dimensional networks are (x_1, x_2), and $((x_1, y_1), (x_2, y_2))$, with the corresponding target populations of $\rho_{target1D-max}$ and $\rho_{target2D-max}$. It can be seen for the presented network parameters that the two-dimensional networks are $O(10^{-2})$ more efficient than the one-dimensional ones.

$[\Gamma_{sink}, V, T, \gamma, \Gamma]$	$\delta\rho_{21}$	$\rho_{sink1D-max}$	$\rho_{sink2D-max}$	x_1, x_2	$(x_1, y_1), (x_2, y_2)$
$\Gamma_{sink}.T = 5, [0.9, 1, 5.56, 0, 0]$	0.009317	0.963611	0.972928	$0.3544, -0.2149$	$(-0.2155, 0.5743)$ $(0.2439, 0.0652)$
$\Gamma_{sink}.T = 5, [1, 1, 5, 0, 0]$	0.011836	0.961117	0.972954	$-0.2305, 0.35448$	$(0.2678, -0.0972)$ $(-0.2322, -0.5275)$
$\Gamma_{sink}.T = 5, [1.1, 1, 4.54, 0, 0]$	0.010636	0.960848	0.971484	-0.2027, 0.3259	$(-0.2388, 0.4764)$ $(0.2905, 0.1208)$
$\Gamma_{sink}.T = 5, [1.2, 1, 4.17, 0, 0]$	0.011700	0.959791	0.971492	0.3350, -0.2052	$(0.2525, -0.0997)$ $(-0.1958, 0.4459)$
$\Gamma_{sink}.T = 5, [1.3, 1, 3.85, 0, 0]$	0.009048	0.961785	0.970833	-0.2051, 0.3388	$(0.2680, -0.0604)$ $(-0.2139, 0.4291)$
$\Gamma_{sink}.T = 5, [1.4, 1, 3.57, 0, 0]$	0.009486	0.959932	0.969419	-0.2092, 0.3462	$(0.2836, -0.0214)$ $(-0.2289, 0.4098)$
$\Gamma_{sink}.T = 5, [5, 1, 1, 0, 0]$	-2.7×10^{-10}	0.848768	0.848768	0.3870, -0.2933	$(0.3870, 0)$ $(-0.2933, 0)$

TABLE A.2: Continuing Table A.1

$[\Gamma_{sink}, V, T, \gamma, \Gamma]$	$\delta\rho_{21}$	$\rho_{sink1D-max}$	$\rho_{sink2D-max}$	x_1, x_2	$(x_1, y_1), (x_2, y_2)$
$\Gamma_{sink}.T = 5, [0.8, 2, 6.25, 0, 0]$	0.002763	0.931620	0.934383	$-0.1896, 0.3330$	$(0.2626, -0.1754)$ $(-0.2313, -0.5654)$
$\Gamma_{sink}.T = 5, [0.7, 2, 7.143, 0, 0]$	0.001789	0.928443	0.930232	$0.2836, -0.1919$	$(0.2535, 0.2033)$, $(-0.2335, 0.6115)$
$\Gamma_{sink}.T = 5, [0.6, 2, 8.33, 0, 0]$	0.000333	0.924352	0.924685	$-0.1921, 0.26944$	$(-0.2231, 0.5594)$, $(0.2497, 0.2023)$
$\Gamma_{sink}.T = 5, [1.2, 2, 4.167, 0, 0]$	0.001410	0.939192	0.940602	$-0.1901, 0.3338$	$(-0.2086, 0.2850)$ $(0.32640, 0.1108)$

TABLE A.3: Continuing Table A.2

$[\Gamma_{sink}, V, T, \gamma, \Gamma]$	$\delta\rho_{21}$	$\rho_{sink1D-max}$	$\rho_{sink2D-max}$	x_1, x_2	$(x_1, y_1), (x_2, y_2)$
$\Gamma_{sink}.V = 0.7, [0.6, 1.167, 7.143, 0, 0]$	0.004385	0.957473	0.961858	$-0.2091, 0.2606$	$(-0.2383, 0.6885)$, $(0.2376, 0.2286)$
$\Gamma_{sink}.V = 0.7, [0.7, 1, 7.143, 0, 0]$	0.012111	0.962097	0.974209	$0.2849, -0.2031$	$(0.2710, -0.2665)$, $(-0.2593, -0.6908)$
$\Gamma_{sink}.V = 0.7, [0.78, 0.9, 7.143, 0, 0]$	0.009820	0.970849	0.980669	$-0.2027, 0.3537$	$(0.2637, -0.1534)$, $(-0.2286, -0.5877)$
$\Gamma_{sink}.V = 0.7, [0.875, 0.8, 7.143, 0, 0]$	0.001245	0.979838	0.981084	$-0.2109, 0.3614$	$(0.3702, -0.3183)$, $(-0.2981, -0.4617)$
$\Gamma_{sink}.V = 0.7, [1, 0.7, 7.143, 0, 0]$	0.001031	0.987718	0.988749	$0.3680, -0.2231$	$(0.3488, 0.1590)$, $(-0.2756, 0.3559)$
$\Gamma_{sink}.V = 0.7, [1.167, 0.6, 7.143, 0, 0]$	0.003868	0.957472	0.961341	$-0.2092, 0.2604$	$(-0.2281, 0.5962)$, $(0.2360, 0.1873)$
$V.T = 7.143, [0.7, 0.8, 8.93, 0, 0]$	0.008702	0.978148	0.986851	$0.3555, -0.1904$	$(-0.2226, -0.6522)$, $(0.2540, -0.1571)$
$V.T = 7.143, [0.7, 1.2, 5.95, 0, 0]$	0.006737	0.951619	0.958356	$0.2725, -0.2101$	$(-0.2289, 0.5704)$, $(0.2442, 0.1647)$
$[0.7; 1; 7; 0; 0.01]$	0.001080	0.920531	0.921611	$0.341386, -0.203263$	$(0.3343, -0.1196)$ $(-0.2240, -0.2834)$
$[0.7, 0.8, 7, 0, 0.01]$	0.006440	0.963963	0.9704029	$0.2689, -0.2048$	$(0.2493, -0.1793)$ $(-0.2240, -0.5357)$

TABLE A.4: This table shows the optimized target population of two and one-dimensional networks. The product of two network parameter in some cases is kept constant. It is shown that for the chosen network parameters the two-dimensional networks are more efficient than the one-dimensional ones.

A.2 Clone configurations of qubit networks

Here we present the optimized target populations of qubit networks with configurations including closely located dipolar sites. To check the accuracy of the calculated sink populations via the $ode15s$ function of *MATLAB* we controlled the trace of the total density matrix of the system and environment up to the 15^{th} decimal digit. This was applied by changing the relative and absolute tolerances of the $ode15s$ function in each case. The relative tolerance of the *ode* solver is the average of acceptable errors for the solutions ($\rho_{vec}(t_{max})$), and the absolute tolerance ($'AbsTol'$) is a vector consisting the maximum acceptable error for each element of $\rho_{vec}(t_{max})$.

In all cases the positions of the first and last sites are fixed at $x_1 = -1, x_4 = 1$ and the network parameters considered for all configurations of Table A.5 are ($\Gamma_{sink} = 0.1, V = 1, \Gamma = 0.01, \gamma = 0, t_{max} = 10$). In the first five rows of Table A.5, the network configuration $(x_1 = -1, x_2, x_3, x_4 = 1)$ is fixed and the distance between the interior sites $O(\delta x_{min})$ decreases from 10^{-5} to 10^{-15}. In the last five rows of Table A.5 the position of the interior sites and their relative distances $O(\delta x_{min})$ change leading to no variation in $\rho_{N+1,N+1}$. The sixth row with $O(\delta x_{min}) = 0.1$ is an example showing that the increase of the pair distance ($O(\delta x_{min})$) can change the target population.

The network parameters of Tables A.6, A.7 are ($\Gamma_{sink} = 1, V = 10, \Gamma = 0.01, \gamma = 0, tmax = 1$), and ($\Gamma_{sink} = 1, V = 10, \Gamma = 0.01, \gamma = 0.5, tmax = 1$), respectively, and in each table the pair position and the pair distance are different. It can be confirmed from Tables A.6, A.7 that the target populations of such networks consisting a pair of sites ($O(\delta x_{min}) < 10^{-3}$) only depend on the network parameters and does not vary according to the position of the interior sites.

x_2, x_3	$O(\delta x_{min})$	$ode(RelTol, AbsTol)$	$Tr(\rho(t_{max}))$	$\rho_{target-max}$
0.179087620299409, 0.179098370635905	10^{-5}	$10^{-12}, 10^{-14}$	1.000000000000000 + 0.000000000000000i	0.345001583975367
0.179087620299409, 0.179086620299409	10^{-6}	$10^{-14}, 10^{-16}$	1.000000000000000 - 0.000000000000000i	0.345001583982857
0.179087620299409, 0.179089620299409	10^{-6}	$10^{-12}, 10^{-14}$	1.000000000000000 + 0.000000000000000i	0.345001583975371
0.179087631299409, 0.179087631399409	10^{-10}	$10^{-12}, 10^{-13}$	1.000000000000000 - 0.000000000000000i	0.345001583974745
0.179087631299409, 0.179087631299408	10^{-15}	$10^{-12}, 10^{-13}$	1.000000000000000 - 0.000000000000000i	0.345001583974745
0.220396956151637, -0.213588601043372	10^{-1}	$10^{-11}, 10^{-12}$	1.000000000000000 - 0.000000000000000i	0.593430042263472
0.220396956151637, 0.220396956151638	10^{-15}	$10^{-13}, 10^{-15}$	1.000000000000000 + 0.000000000000000i	0.345001583982032
0.220396956151637, 0.220396946141637	10^{-11}	$10^{-13}, 10^{-15}$	1.000000000000000 - 0.000000000000000i	0.345001583982033
0.510000001, 0.510000002	10^{-9}	$10^{-13}, 10^{-15}$	1.000000000000000 - 0.000000000000000i	0.345001583982036
0.3100001, 0.3100002	10^{-7}	$10^{-13}, 10^{-14}$	1.000000000000000 - 0.000000000000000i	0.345001583981941
-0.710000, -0.710001	10^{-6}	$10^{-14}, 10^{-15}$	1.000000000000000 + 0.000000000000000i	0.345001583981941

TABLE A.5: This table shows the exact target population of four-site networks including two closely located sites. The network parameters of all cases are $\Gamma_{target} = 0.1, V = 1, \Gamma = 0.01, \gamma = 0, tmax = 10$. ρ_{target} is the target population where the network configuration is denoted as $(x_1 = -1, x_2, x_3, x_4 = 1)$. $O(\delta x_{min})$ is the approximate distance between the interior sites, and $Tr(\rho(t_{max}))$ shows the trace of final density matrix of the system up to 15^{th} decimal digit. The relative and absolute tolerances of $ode15$ solver are adjusted for each case to maintain the accuracy of the trace of the density matrix. The maximum calculation time of each case was 1 second.

x_2, x_3	$O(\delta x_{min})$	$ode(RelTol, AbsTol)$	$Tr(\rho(t_{max}))$	$\rho_{target-max}$
-0.20000, -0.20001	10^{-5}	$10^{-12}, 10^{-14}$	1.000000000000000 + 0.000000000000000i	0.389802667849927
0.6000, 0.6001	10^{-4}	$10^{-12}, 10^{-12}$	1.000000000000000 - 0.000000000000000i	0.389802667795225
0.0000006, 0.0000007	10^{-7}	$10^{-12}, 10^{-12}$	1.000000000000000 - 0.000000000000000i	0.389802667829627
0.300, 0.301	10^{-3}	$10^{-10}, 10^{-10}$	1.000000000002080 - 0.000000000000000i	0.389802654705071

TABLE A.6: Network parameters of all cases is considered as $\Gamma_{target} = 1, V = 10, \Gamma = 0.01, \gamma = 0, tmax = 1$. ρ_{target} is the target site population of the network of site configuration $(x_1 = -1, x_2, x_3, x_4 = 1)$. $O(\delta x_{min})$ is the approximate distance between the middle sites, and $Tr(\rho(t_{max}))$ represents the trace of final density matrix of the system. the relative and absolute tolerances of $ode15$ solver are adjusted in each case to maintain the trace accuracy and a maximum calculation time of 1 second.

x_2, x_3	$O(\delta x_{min})$	$ode(RelTol, AbsTol)$	$Tr(\rho(t_{max}))$	$\rho_{target-max}$
0.000079, 0.000080	10^{-6}	$10^{-12}, 10^{-17}$	1.000000000000000 + 0.000000000000000i	0.322131771753089
0.3000334, 0.3000334	10^{-7}	$10^{-12}, 10^{-17}$	1.000000000000000 + 0.000000000000000i	0.322131771752234
0.0000006, 0.0000007	10^{-7}	$10^{-12}, 10^{-15}$	1.000000000000000 - 0.000000000000000i	0.322131771751857
0.300, 0.301	10^{-3}	$10^{-10}, 10^{-10}$	1.000000000000410 + 0.000000000000000i	0.322131760527033

TABLE A.7: Network parameters of all cases is considered as $\Gamma_{target} = 1, V = 10, \Gamma = 0.01, \gamma = 0.5, tmax = 1$ is the target site population of the network of site configuration $(x_1 = -1, x_2, x_3, x_4 = 1)$. $O(\delta x_{min})$ is the approximate distance between the middle sites, and $Tr(\rho(t_{max}))$ represents the trace of final density matrix of the system. the relative and absolute tolerances of $ode15$ solver are adjusted in each case to maintain the trace accuracy and a maximum calculation time of 1 second.

References

[1] C. Javaherian and B. Shokri. *Guided dispersion characteristics of metallic single-wall carbon nanotubes*. J. Phys. D. Appl. Phys. **42**, 055307 (2009).

[2] Y. Ahmadizadeh, C. Javaherian, and B. Shokri. *Study of geometrical effects on the characteristics of metallic double-walled carbon nanotube waveguides through quantum hydrodynamics*. Phys. Plasma **16**, 063501 (2009).

[3] Y. Ahmadizadeh, C. Javaherian, and B. .Shokri. *Response to comment on study of geometrical effects on the characteristics of metallic double-walled carbon nanotube waveguides through quantum hydrodynamics[phys. plasmas16, 084703 (2009)].* Phys. Plasmas **16**, 084704 (2009).

[4] B. S. M Nejati, C. Javaherian and B. Jazi. *The single-wall carbon nanotube waveguides and excitation of their $\sigma + \pi$ plasmons by an electron beam.* Phys. Plasmas **16**, 2108 (2009).

[5] M. Nejati, C. Javaherian, B. Shokri, and B. Jazi. *Response to "comment on 'the single-wall carbon nanotube waveguides and excitation of their $\sigma + \pi$ plasmons by an electron beam'"[phys. plasmas 16, 054705 (2009)].* Phys. Plasmas **16**, 054706 (2009).

[6] M. Nejati, C. Javaherian, B. Shokri, and B. Jazi. *Erratum: "the single-wall carbon nanotube*

waveguides and excitation of their $\sigma + \pi$ plasmons by an electron beam" [phys. plasmas 16, 022108 (2009)]. Phys. Plasmas **16**, 9901 (2009).

[7] M. Ramm, T. Pruttivarasin, and H. Haffner. *Energy transport in trapped ion chains*. New J. Phys. **16**, 063062 (2014).

[8] S. Maier, P. G. Kik, L. A. Sweatlock, H. A. Atwater, J. J. Penninkhof, A. Polman, S. Meltzer, A. A. G. R. E. Harel, and B. E. Koel. *Energy transport in metal nanoparticle plasmon waveguides*. Mat. Res. Soc. Symp. Proc. **777**, T.7.1.1 (2003).

[9] F. R. Braakman, P. Barthelemy, C. Reichl, W. Wegscheider, and L. M. K. Vandersypen. *Long-distance coherent coupling in a quantum dot array*. Nat. Nanotech. **8**, 432 (2013).

[10] Y. V. Nazarov and Y. M. Blanter. *Quantum transport, introduction to nanoscience*. Cambridge University Press (2009).

[11] S. Datta. *Quantum transport: Atom to transistor*. Cambridge University Press (2005).

[12] E. Vetsch, D. Reitz, G. Sague, R. Schmidt, S. T. Dawkins, and A. Rauschenbeutel. *Optical interface created by laser-cooled atoms trapped in the evanescent field surrounding an optical nanofiber*. Phys. Rev. L. **104**, 203603 (2010).

[13] K. Hammerer, A. S. Sorensen, and E. S. Polzik. *Quantum interface between light and atomic ensembles*. Rev. Mod. Phys. **82**, 1041 (2010).

[14] A. Reiserer and G. Rempe. *Cavity-based quantum networks with single atoms and optical photons*. Accepted in Rev. Mod. Phys. (2015).

[15] S. Bose. *Quantum Communication through an Unmodulated Spin Chain*. Phys. Rev. L. **91**, 207901 (2003).

[16] M. Christandl, N. Datta, A. Ekert, and A. Landahl. *Perfect State Transfer in Quantum Spin Networks*. Phys. Rev. L. **92**, 187902 (2004).

[17] M. Tame, M. Paternostro, M. Kim, and V. Vedral. *Quantum-information processing with noisy cluster states*. Phys. Rev. A **72**, 012319 (2005).

[18] T. Osborne and N. Linden. *Propagation of quantum information through a spin system*. Phys. Rev. A **69**, 052315 (2004).

[19] D. Burgarth and S. Bose. *Conclusive and arbitrarily perfect quantum-state transfer using parallel spin-chain channels*. Phys. Rev. A **71**, 052315 (2005).

[20] D. Burgarth, S. Bose, and V. Giovannetti. *Efficient and Perfect State Transfer in Quantum Chains*. Int. J. Quantum Inf. **04**, 405 (2006).

[21] E. Townsend, A. Debrecht, and G. W. Bryant. *Approaching the quantum limit for nanoplasmonics*. J. Mat. Res. **30**, 2389 (2015).

[22] D. Loss and D. P. DiVincenzo. *Quantum computation with quantum dots*. Phys. Rev. L. **57**, 120 (1998).

[23] H. P. Breuer and F. Petruccione. *The theory of open quantum systems*. OUP Oxford 2007 (2002).

[24] Y. Liu, W. Cheng, Z. Y. Gao, and H. S. Zeng. *Environmental coherence and excitation effects in non-markovian dynamics*. Q. Inf. and Comp. **23**, 23021 (2015).

[25] X. Zhao, J. Jing, J. Q. You, and T. Yu. *Dynamics of coupled cavity arrays embedded in a non-markovian bath*. Q. Inf. and Comp. **14**, 741 (2014).

[26] F. Caruso, a. W. Chin, A. Datta, S. F. Huelga, and M. B. Plenio. *Highly efficient energy excitation transfer in light-harvesting complexes: The fundamental role of noise-assisted transport*. J. Chem. Phys. **131**, 105106 (2009).

[27] M. Znidaric and M. Horvat. *Transport in a disordered tight-binding chain with dephasing*. Eur. Phys. J. B **86**, 67 (2013).

[28] F. Caruso, N. Spagnolo, C. Vitelli, F. Sciarrino, and M. B. Plenio. *Simulation of noise-assisted transport via optical cavity networks*. Phys. Rev. A **83**, 013811 (2011).

[29] K. L. Brown, W. J. Munro, and V. Kendon. *Environmental coherence and excitation effects in non-markovian dynamics*. Entropy **12**, 2268 (2010).

[30] V. S. M. P. Kumar, S. A. Malinovskaya. *Optimal control of population and coherence in three-level systems*. J. Phys. B: At. Mol. Opt. Phys **44**, 154010 (2011).

[31] L. M. Jong, D. Greentree, V. I. Conrad, L. C. L. Hollenberg, and D. N. Jamieson. *Coherent tunneling adiabatic passage with the alternating coupling scheme.* Nanotechnol. **20**, 405402 (2009).

[32] B. K. Andrew D. Greentree. *Dark-state adiabatic passage with spin-one particles*. Phys. Rev. A **90**, 012319 (2014).

[33] S. Oh, Y. P. Shim, J. Fei, M. Friesen, and X. Hu. *Resonant adiabatic passage with three qubits*. Phys. Rev. A **87**, 022332 (2013).

[34] T. Brandes and F. Renzoni. *Current switch by coherent trapping of electrons in quantum dots*. Phys. Rev. L. **85**, 4148 (2000).

[35] K. Eckert, M. Lewenstein, R. Corbalan, G. Birkl, W. Ertmer, and J. Mompart. *Three-level atom optics via the tunneling interaction*. Phys. Rev. A **70**, 023606 (2004).

[36] A. D. Greentree, J. H. Cole, A. R. Hamilton, and L. C. L. Hollenberg. *Coherent electronic transfer in quantum dot systems using adiabatic passage*. Phys. Rev. B **70**, 235317 (2004).

[37] M. Rab, J. H. Cole, N. G. Parker, A. D. Greentree, L. C. L. Hollenberg, and A. M. Martin. *Spatial coherent transport of interacting dilute bose gases*. Phys. Rev. A **77**, 061602 (2008).

[38] E. Paspalakis. *Adiabatic three-waveguide directional coupler*. Opt. Commun. **30**, 258 (2006).

[39] C. J. Bradly, M. Rab, a. D. Greentree, and a. M. Martin. *Coherent tunneling via adiabatic passage in a three-well Bose-Hubbard system*. Phys. Rev. A **85**, 053609 (2012).

[40] L. Tian. *Energy transport in metal nanoparticle plasmon waveguides*. Phys. Rev. L. **105**, 167001 (2010).

[41] T. G. Tiecke, J. D. Thompson, N. P. de Leon, L. R. Liu, V. Vuleti, and M. D. Lukin. *Nanophotonic quantum phase switch with a single atom*. Nature **508**, 241 (2014).

[42] B. H. Nguyen and V. H. Nguyen. *Engineered spin chains for perfect quantum state transfer*. Adv. Nat. Sci.: Nanosci. Nanotechnol. **1**, 039802 (2010).

[43] B. Vaucher, D. Burgarth, and S. Bose. *Arbitrarily perfect quantum communication using unmodulated spin chains, a collaborative approach*. J. Opt. B: Q. and Semiclass. Opt. **7**, S356 (2005).

[44] R. Blatt and D. Wineland. *Entangled states of trapped atomic ions*. Nat. **453**, 1008 (2008).

[45] D. J. Wineland, C. Monroe, W. M. Itano, D. Leibfried, B. E. King, and D. M. Meekhof. *Experimental issues in coherent quantum-state manipulation of trapped atomic ions*. J. Res. Natl. Inst. Stand. Technol. **103**, 259 (1998).

[46] A. Lyakhov and C. Bruder. *Quantum state transfer in arrays of flux qubits*. New Journal of Physics **7**, 181 (2005).

[47] J. Q. You and F. Nori. *Atomic physics and quantum optics using superconducting circuits*. Nature **474**, 589 (2011).

[48] H. Wei and H. Xu. *Nanowire-based plasmonic waveguides and devices for integrated nanophotonic circuits*. Nanophotonics **1**, 155 (2012).

[49] S. Raza, N. Stenger, A. Pors, T. Holmgaard, S. Kadkhodazadeh, J. B. Wagner, K. Pedersen, M. Wubs, S. I. Bozhevolnyi, and N. A. Mortensen. *Extremely confined gap surface-plasmon modes excited by electrons*. Nat. Commun. **82**, 1 (2014).

[50] D. K. Gramotnev, M. G. Nielsen, S. J. Tan, M. L. Kurth, and S. I. Bozhevolnyi. *Gap surface plasmon waveguides with enhanced integration and functionality*. Nano Let. **12**, 359 (2012).

[51] K. Tanaka and M. Tanaka. *Simulations of nanometric optical circuits based on surface plasmon polariton gap waveguide*. Appl. Phys. Let. **82**, 1158) (2003).

[52] B. Wang and G. P. Wang. *Surface plasmon polariton propagation in nanoscale metal gap waveguides*. Opt. Let. **29**, 1992 (2004).

[53] L. Wang and R. Renner. *One-shot classical-quantum capacity and hypothesis testing*. Phys. Rev. L. **108**, 200501 (2012).

[54] J. M. Renes and R. Renner. *One-shot classical data compression with quantum side information and the distillation of common randomness or secret keys*. IEEE Transections on Information Theory **58**, 1985 (2012).

[55] M. H. G. S. L. Fernando, M. Brandao. *An area law for entanglement from exponential decay of correlations*. Rev. Mod. Phys. **9**, 721 (2013).

[56] J. Eisert, M. Cramer, and M. Plenio. *Colloquium: Area laws for the entanglement entropy*. Rev. Mod. Phys. **82**, 277 (2010).

[57] T. Scholak, T. Wellens, and A. Buchleitner. *Optimal networks for excitonic energy transport*. J. Phys. B At. Mol. Opt. Phys. **44**, 184012 (2011).

[58] A. Kay. *Perfect state transfer: Beyond nearest-neighbor couplings*. Phys. Rev. A **73**, 032306 (2006).

[59] D. Mogilevtsev, a. Maloshtan, S. Kilin, L. E. Oliveira, and S. B. Cavalcanti. *Spontaneous emission and qubit transfer in spin-1/2 chains*. J. Phys. B At. Mol. Opt. Phys. **43**, 095506 (2010).

[60] Z. Song. *Quantum information storage and state transfer based on spin systems*. Low Temp. Phys. **31**, 686 (2005).

[61] H. P. Breuer and F. Petruccione. *The theory of open quantum systemss*. Oxford University Press (2007).

[62] P. Walther, K. J. Resch, T. Rudolph, E. Schenck, H. Weinfurter, V. Vedral, M. Aspelmeyer, and A. Zeilinger. *Experimental one-way quantum computing*. Nature **434**, 169 (2005).

[63] A. S. Green and T. Altenkirch. *From reversible to irreversible computations*. Electronic Notes in Theoretical Computer Science **210**, 65 (2008).

[64] D. Leibfried, E. Knill, C. Ospelkaus, and D. Wineland. *Transport quantum logic gates for trapped ions*. Phys. Rev. A **76**, 032324 (2007).

[65] S. a. Maier, P. G. Kik, and H. a. Atwater. *Observation of coupled plasmon-polariton modes in Au nanoparticle chain waveguides of different lengths: Estimation of waveguide loss*. Appl. Phys. Lett. **81**, 1714 (2002).

[66] A. Zwick, G. a. Álvarez, J. Stolze, and O. Osenda. *Robustness of spin-coupling distributions for perfect quantum state transfer*. Phys. Rev. A **84**, 022311 (2011).

[67] a. W. Chin, a. Datta, F. Caruso, S. F. Huelga, and M. B. Plenio. *Noise-assisted energy transfer in quantum networks and light-harvesting complexes*. New J. Phys. **12**, 065002 (2010).

[68] M. B. Plenio and S. F. Huelga. *Dephasing-assisted transport: quantum networks and biomolecules*. New J. Phys. **10**, 113019 (2008).

[69] P. Rebentrost, M. Mohseni, I. Kassal, S. Lloyd, and A. Aspuru-Guzik. *Environment-assisted quantum transport*. New J. Phys. **11**, 033003 (2009).

[70] D. de Falco and D. Tamascelli. *Noise-assisted quantum transport and computation*. J. Phys. A Math. Theor. **46**, 225301 (2013).

[71] N. Wakamiya, K. Leibnitz, and M. Murata. *Noise-assisted control in information networks*. 2007 Front. Converg. Biosci. Inf. Technol. p. 833 (2007).

[72] A. Marais, I. Sinayskiy, A. Kay, F. Petruccione, and A. Ekert. *Decoherence-assisted transport in quantum networks*. New J. Phys. **15**, 013038 (2013).

[73] J. W. Britton, B. C. Sawyer, A. C. Keith, C.-C. J. Wang, J. K. Freericks, H. Uys, M. J. Biercuk, and J. J. Bollinger. *Engineered two-dimensional Ising interactions in a trapped-ion quantum simulator with hundreds of spins.* Nature **484**, 489 (2012).

[74] G. Vidal and R. F. Werner. *Computable measure of entanglement*. Phys. Rev. A **65**, 032314 (2002).

[75] M. B. Plenio. *Logarithmic negativity: A full entanglement monotone that is not convex*. Phys. Rev. L. **95**, 090503 (2005).

[76] J. Cirac, P. Zoller, H. Kimble, and H. Mabuchi. *Quantum State Transfer and Entanglement Distribution among Distant Nodes in a Quantum Network*. Phy. Rev. L. **78**, 3221 (1997).

[77] H. J. Kimble. *The quantum internet*. Nature **453**, 1023 (2008).

[78] J. Volz and A. Rauschenbeutel. *Triggering an optical transistor with one photon.* Sci. Appl. Phys. **341**, 725 (2013).

[79] T. Hira, T. Homma, T. Uchiyama, K. Kuwamura, and T. Saiki. *Switching of localized surface plasmon resonance of gold nanoparticles on a GeSbTe film mediated by nanoscale phase change and modification of surface morphology*. Appl. Phys. L. **103**, 241101 (2013).

[80] J. D. Cox, M. R. Singh, C. von Bilderling, and A. V. Bragas. *A Nonlinear Switching Mechanism in Quantum Dot and Metallic Nanoparticle Hybrid Systems*. Advanced Optical Materials **1**, 460 (2013).

[81] Z. Lian, P. Horak, X. Feng, L. Xiao, K. Frampton, N. White, J. a. Tucknott, H. Rutt, D. N. Payne, W. Stewart, and W. H. Loh. *Nanomechanical optical fiber.* Opt. exp. **20**, 29386 (2012).

[82] J.-J. Li and K.-D. Zhu. *A tunable optical Kerr switch based on a nanomechanical resonator coupled to a quantum dot.* Nanotechnol. **21**, 205501 (2010).

[83] M. M. Maye, M. T. Kumara, D. Nykypanchuk, W. B. Sherman, and O. Gang. *Switching binary states of nanoparticle superlattices and dimer clusters by DNA strands.* Nat. nanotechnol. **5**, 116 (2010).

[84] J. Merlein, M. Kahl, A. Zuschlag, A. Sell, A. Halm, J. Boneberg, P. Leiderer, A. Leitenstorfer, and R. Bratschitsch. *Nanomechanical control of an optical antenna*. Nat. Photonics **2**, 230 (2008).

[85] C. Javaherian and J. Twamley. *Robustness of optimal transport in one dimensional particle quantum networks*. Phys. Rev. A **90**, 042313 (2014).

[86] A. B. O. Mülken. *Continuous-time quantum walks: Models for coherent transport on complex networks*. Phy. Rep. **502**, 37 (2011).

[87] A. B. E. Agliari and O. Mülken. *Quantum-walk approach to searching on fractal structures*. Phy. Rev. A **82**, 012305 (2010).